

Journal of Geophysical Research: Oceans

RESEARCH ARTICLE

10.1002/2015JC011325

Key Points:

- Model study of individual and combined impact of river and rain on stratification and circulation
- Model study of individual and combined impact of river and rain on stratification and circulation
- Contrasting response of SST in the western and eastern Bay of Bengal explained

Correspondence to:

P. N. Vinayachandran,
vinay@caos.iisc.ernet.in

Citation:

Behara, A., and P. N. Vinayachandran (2016), An OGCM study of the impact of rain and river water forcing on the Bay of Bengal, *J. Geophys. Res. Oceans*, 121, doi:10.1002/2015JC011325.

Received 18 SEP 2015

Accepted 14 MAR 2016

Accepted article online 18 MAR 2016

An OGCM study of the impact of rain and river water forcing on the Bay of Bengal

Ambica Behara¹ and P. N. Vinayachandran¹

¹Centre for Atmospheric and Oceanic Sciences, Indian Institute of Science, Bangalore, India

Abstract Individual and combined effects of rainfall and river discharge on the Bay of Bengal (BoB) is investigated using an Ocean General Circulation Model. A set of four sensitivity experiments, forced with same air-sea heat flux, but retaining either river runoff or rainfall or both is carried out. These experiments show that the river water is exported out of the bay along the western boundary during winter and rain water along the eastern boundary during summer. Runoff leads to a large (>3 psu) decrease in salinity in the northern bay during summer and along the western boundary during winter, with a weaker contribution from rainfall. The sea surface temperature response to freshwater forcing shows large spatial variations with eastern bay showing higher differences. The northwestern bay warms by $\sim 1.5^{\circ}\text{C}$ in the presence of freshwater during summer, due to greater heat absorption within a shallow mixed layer (ML). This warming is caused in nearly equal proportions by rain and river water in early summer, but the contribution by river water dominates during peak and withdrawal phases of the summer monsoon. Northeastern bay, in contrast, is cooler by $1.5\text{--}3^{\circ}\text{C}$ in the presence of freshwater, caused primarily by river runoff, owing to the winter cooling over a thin ML. Temperature inversions form due to surface cooling of a river stratified layer during winter in the northwestern bay and due to radiation penetrating below the ML during summer in the northeastern bay.

1. Introduction

The special feature that distinguishes the Bay of Bengal (BoB or bay) from the rest of the Indian Ocean is that it receives large quantity of freshwater from rainfall and discharge by several rivers. Owing to the enormous freshwater input, the salinity of the upper layer of the bay is remarkably low resulting in strong vertical stratification [Shetye et al., 1991, 1996; Vinayachandran et al., 2002; Rao and Sivakumar, 2003; Yu and McPhaden, 2011; Chaitanya et al., 2014a,b], thereby influencing dynamics and thermodynamics of the mixed layer (ML). River discharge lowers the salinity near the river mouths and coastal regions along its pathway, whereas precipitation is distributed over a much larger area. The individual as well as combined impact of precipitation and river discharge on the dynamics and thermodynamics of the BoB is the topic of this study.

The northern bay, unlike the Arabian Sea, maintains a warm sea surface temperature (SST), $>28^{\circ}\text{C}$, throughout the summer or southwest monsoon (SWM) [Vinayachandran and Shetye, 1991], and provides favorable conditions for the development of several low pressure systems through the season. The maintenance of this warmer SST in the BoB has been attributed to the low salinity cap [Shenoi et al., 2002]. The BoB mixed layer depth (MLD) is determined more by the isohaline layer than by the isothermal layer. Therefore, the ML is rather thin during the summer monsoon even when the winds are strong. Shoaling of the ML is crucial for warming the SST after the passing of each monsoon weather system. Therefore, understanding the impact of freshwater on the thermodynamics of the upper layer of the BoB forms an essential component of air-sea interaction studies related to monsoon.

The layer between the top of the thermocline and the base of the ML is termed as the barrier layer [Lukas and Lindstrom, 1991; Sprintall and Tomczak, 1992], for it can inhibit cooling of an entraining ML. Freshening of the near surface layer can lead to barrier layer formation, and therefore affect mixed layer thermodynamics. The isothermal layer, in such situations, is deeper compared to the isohaline and the isopycnal layer. A ML that is insulated from cooling by entrainment in presence of net air-sea heat flux directed to the ocean, warms rapidly. Using a 1-D ocean model, Miller [1976] showed that shoaling of the ML due to salinity stratification can warm or cool the upper ocean depending on the air-sea heat fluxes and entrainment at the interface between the ML and the layer below.

The influence of surface salinity variability on the formation of barrier layer in the BoB [Vinayachandran *et al.*, 2002; Girishkumar *et al.*, 2011] and its impact on the SST has been evaluated by observational [Yu and McPhaden, 2011; Girishkumar *et al.*, 2013] and modeling studies [Han *et al.*, 2001; Howden and Murtugudde, 2001; Seo *et al.*, 2009; Vinayachandran *et al.*, 2012; Durand *et al.*, 2007]. Han *et al.* [2001], using a $4\frac{1}{2}$ -layer reduced gravity model, found that the effect of freshwater is prominent only in the northwestern BoB with an SST increase of about $0.5\text{--}1^{\circ}\text{C}$, which was caused by the river discharge. The freshwater input strengthened the east India coastal current (EICC) by 0.1 ms^{-1} in their layered model. Howden and Murtugudde [2001] found that river discharge in their model increased the SST by 1°C close to the river mouths during summer, but the annual SST averaged over the BoB (away from the river mouths) decreased by 0.1°C . This decrease in SST due to river discharge was attributed to the shoaling of the ML that caused greater loss of shortwave penetration below the ML and “effective” entrainment due to the presence of cooler waters below the shallow ML. Seo *et al.* [2009] used a regional coupled model in which river effects were mimicked by surface salinity relaxation, and found that salinity stratification caused warming of about 0.1°C during summer and a cooling of 1.1°C during winter averaged over the bay. These differences were as high as 3°C off the river mouths of Ganga and Brahmaputra.

In this paper, we have examined the individual and combined impact of rainfall and river discharge on sea surface salinity (SSS), currents, freshwater transport, SST, and temperature inversion (TI) using an ocean general circulation model (OGCM), which offers refinement in many aspects compared to models used in previous studies. In order to isolate the role of oceanic processes on SST, air-sea heat flux is maintained to be the same in all experiments. We find, most significantly, that eastern and western parts of the bay responds differently to freshwater input during both summer and winter. Details of the model and experiments are presented in section 2 and the model evaluation in section 3. Detailed description of results of experiments for determination of the impact of freshwater forcing is given in section 4. Formation of TI in the presence of freshwater inputs is discussed in section 5 and the summary and conclusions are presented in section 6.

2. The Model

The Indian Ocean model used in this study is based on the Geophysical Fluid Dynamics Laboratory Modular Ocean Model (MOM4p1) [Griffies *et al.*, 2009], and its configuration is similar to that used by Kurian and Vinayachandran [2007] and Vinayachandran *et al.* [2007]. A brief description of the model configuration is given below.

The model has a uniform horizontal resolution of 0.25° and its domain is bounded by latitudes 30°S and 30°N and longitudes 30°E to 120°E . The bottom topography is based on improved version [Sindhu *et al.*, 2007] of ETOPO5 [National Geophysical Data Center, 1988]. The model grid has 40 vertical levels with upper 60 m having a spacing of 5 m and the first grid point is located at 2.5 m depth. Below 60 m depth, the grid spacing increases gradually to a depth of 5000 m. The minimum depth in the model is set to 30 m and grids shallower than 30 m are set to be land points. The northern and western boundaries of the model domain are treated as solid walls. Temperature and salinity are restored to climatological values [Locarnini *et al.*, 2010; Antonov *et al.*, 2010] within sponge layers of width 3.5° , with a time scale of 30 days, near the southern and eastern boundaries. In order to maintain an appropriate influx of saline water masses into the Arabian Sea, sponge layers have also been applied to Red Sea and Persian Gulf [Schiller and Godfrey, 2003].

The equation of state used in the model is based on Jackett *et al.* [2006]. Horizontal mixing is based on Chassignet and Garraffo [2001], tracer physics includes Redi neutral diffusion [Griffies *et al.*, 1998] and Gent-McWilliams stirring using the skew-flux method [Griffies, 1998] combined with Fox-Kemper and Ferrari [2008] and Fox-Kemper *et al.* [2008] submesoscale closure scheme discussed in Griffies *et al.* [2009]. Vertical mixing uses the KPP scheme [Large *et al.*, 1994] with nonlocal mixing. The model uses tidal speed data obtained from Oregon State University Tidal Inversion Software [Egbert and Erofeeva, 2002; Egbert *et al.*, 1994] to calculate the vertical diffusivity and viscosity based on two dissipation mechanisms: one from internal wave breaking [Simmons *et al.*, 2004] and the other from barotropic tides feeling the bottom drag [Lee *et al.*, 2006]. For the calculation of shortwave penetration into the upper ocean, the chlorophyll-based scheme [Morel and Antoine, 1994] has been used. UNESCO SAGE river data set for major rivers along the coasts of India and Sri Lanka is used to force the model (Table 1). Due to the absence of runoff data for Irrawaddy river in the UNESCO data set, Global Runoff Data Center (GRDC) river discharge data for Irrawaddy river has been

Table 1. Climatological Model Forcing^a

Field	Data Source	References	Frequency
Air temperature (K)	NCEP	<i>Kalnay et al. [1996]</i>	Daily
Longwave radiation (Wm^{-2})			
Shortwave radiation (Wm^{-2})			
Specific humidity (kg/kg)			
Wind stress (Nm^{-2})	QuikSCAT	www.ifremer.fr/cersat/en/data/data.htm	
Wind speed (ms^{-1})			
Rainfall rate (ms^{-1})	TRMM	http://daac.gsfc.nasa.gov/precipitation	
River discharge (ms^{-1})	SAGE (UNESCO)	<i>Vörösmarty et al. [1996]</i>	Monthly
Irrawaddy river discharge (ms^{-1})	GRDC	<i>Fekete et al. [2002]</i>	Monthly
Tide velocity (ms^{-1})	OTIS	<i>Egbert and Erofeeva [2002]</i>	
Chlorophyll (mgm^{-3})	SeaWiFS	http://disc.sci.gsfc.nasa.gov/giovanni	

^aClimatology of QuickSCAT wind fields, TRMM precipitation, and NCEP reanalysis data sets have been calculated for the period 2000–2008. The Bulk model is forced with downwelling longwave and shortwave radiations.

used. River discharge is distributed over a horizontal area proportional to the rate of discharge (Figure 1, bottom), within the upper 20 m of the ocean. Rivers with smaller discharge area are either combined together or distributed adjacent to the nearest major river to form a single river system (see Figure 1, bottom).

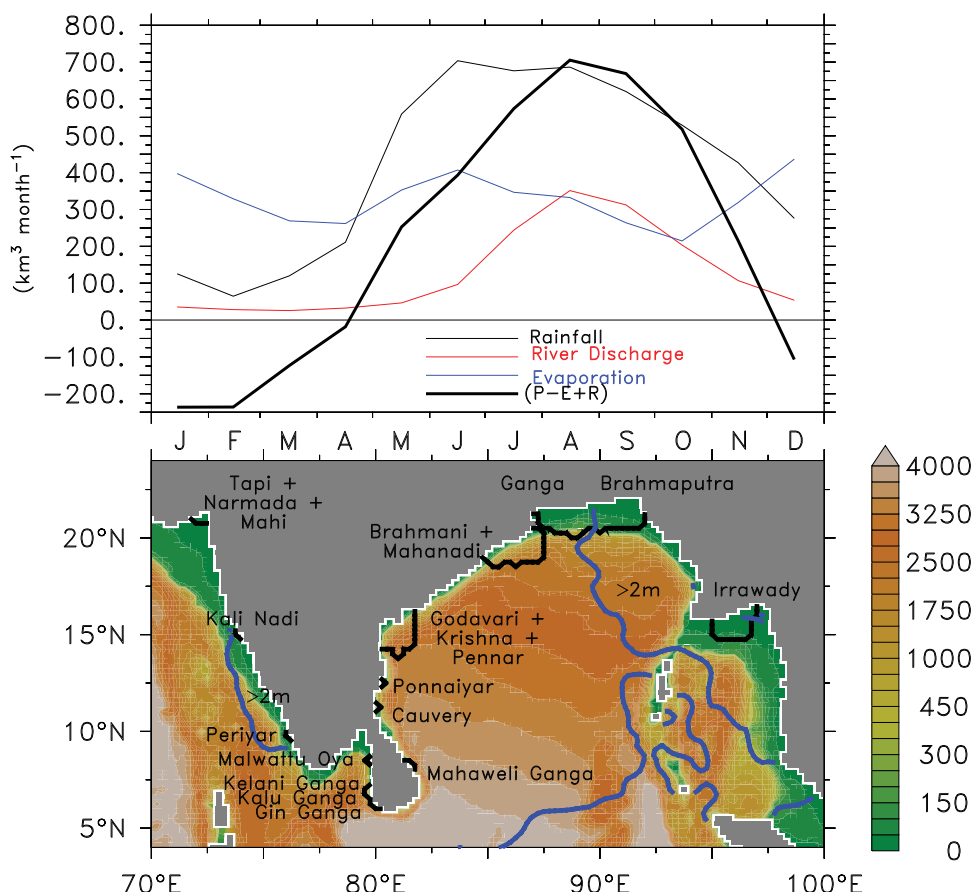


Figure 1. (top) The annual cycle of monthly mean precipitation (black line), evaporation (blue), and river discharge (red) integrated north of 6°N from 80°E to 100°E in $\text{km}^3 \text{ month}^{-1}$. Monthly mean of precipitation (P) is calculated from TRMM, evaporation rate (E) from GSSTFMC monthly climatology, and monthly river runoff (R) data from *Dai and Trenberth [2002]*. The dashed line shows the freshwater flux ($P-E+R$) into the BoB in $\text{km}^3 \text{ month}^{-1}$ estimated from the above data sets. (bottom) The distribution of river discharge in the model. The shading with color scale to the right of the plot shows the topography (m) of the BoB and the white line represents the coastline. The black and blue contours represent the spread of river during the peak discharge time (August–September) and the area over which the total annual rainfall is 2 m (boxcar smoothed by three grid points), respectively. All climatologies are for the period 2000–2008.

2.1. Experiments

The model was started from a state of rest and climatological temperature and salinity for the month of April [Locarnini *et al.*, 2010] as initial conditions and integrated for a period of 9 years using daily climatology (2000–2008) of atmospheric forcing (Table 1). The latent and sensible heat fluxes and outgoing longwave radiation in this run (called BULK run) were calculated based on a bulk formulation [Large and Yeager, 2004], which uses model SST.

The air-sea heat flux from the 9th year of the BULK run was used to force the model for another 10 years. This experiment, retaining both rainfall and river discharge, is given the acronym as WRR (with rain and river). All other data sets used for forcing the WRR are the same as in BULK (Table 1). Three sensitivity experiments were carried out to investigate freshwater forcing of the BoB, namely, WRAIN (with rain and without river), WRIVER (with river and without rain), and NORR (without rain and river). Subtracting the outputs of these sensitivity runs from NORR is considered to give the contribution of individual as well as the composite effect of river discharge and precipitation. Thus, WRAIN–NORR and WRIVER–NORR gives the contribution of rain and river runoff respectively, whereas WRR–NORR gives the combined effect of river and rain. First year output of the sensitivity experiments with same initial conditions capture the immediate response of SST to the freshwater input. However, it takes more than one year to remove all the freshwater that bay receives in a given year. Therefore, the experiments were run for 10 years. Climatologies of the last 5 year outputs of WRR were used for the validation with observations. Last 5 year runs of the sensitivity experiments were used to understand the processes.

Rainfall over the BoB is maximum during July–August, whereas river runoff [Dai and Trenberth, 2002] is maximum during August–September and the annual river discharge (R) into the bay is estimated to be 1537 km^3 . Monthly climatology of evaporation obtained from Goddard Satellite-Based Surface Turbulent Fluxes Monthly Climatology (GSSTFMC) [Shie *et al.*, 2012] shows that the evaporation rate has a semiannual cycle with its first maxima during May–June and the second during December–January. The annual evaporation (E) is estimated to be about 3931 km^3 . Using Tropical Rainfall Measuring Mission (TRMM) data, the annual rainfall (P) in the BoB is estimated to be about 5000 km^3 . Hence, the BoB freshwater input ($P-E+R$) is about 2605 km^3 annually. Freshwater loss due to evaporation is low throughout the year except during winter (Figure 1, top), and freshwater input is maximum during summer (Figure 1, top). Since the primary focus of this study is the monsoons, we have not examined the explicit role of evaporation.

3. The Model Seasonal Cycle

The climatological seasonal cycle of the model for the Indian Ocean has been evaluated by Kurian and Vinayachandran [2007]. Below we present a brief comparison of the WRR simulation for the BoB. Climatology of observational data sets of rainfall, evaporation, and surface currents for the period 2000–2008 have been used for comparison. Monthly climatology of model outputs and observational data sets are used to calculate the annual root mean square error (RMSE) and standard deviation of SSS and SST.

3.1. SSS

Figure 2 compares simulated SSS of the model with that of climatology [Chatterjee *et al.*, 2012], hereafter referred to as NIOclim. A low salinity pool (<31 psu) confined to the northern and northeastern boundary of the BoB during the summer monsoon is present in both NIOclim and WRR. Observational studies by Shetye *et al.* [1996]; Vinayachandran *et al.* [2002] reported the presence of a freshwater plume that flows southward during summer in the head bay and pushed offshore around 20°N . This freshwater plume and its offshore drift found in several modeling studies [Han and McCreary, 2001; Howden and Murtugudde, 2001; Vinayachandran and Nanjundiah, 2009; Akhil *et al.*, 2014] is well reproduced in our model (Figure 2, September).

The realistic freshwater forcing enables the model to simulate low salinity pools in the bay, but the model salinity is higher, particularly near the river mouths where the RMSE of model surface salinity is greater than 2 (Figure 4f) with respect to NIOclim. This difference is most probably due to deficiencies in the runoff data set. The increase in surface salinity from head bay toward south [Rao and Sivakumar, 2003; Vinayachandran *et al.*, 2013] is well reproduced in the model. The annual standard deviation of SSS in NIOclim (Figure 4c) shows that the BoB exhibits maximum variation to the north of 15°N . The model captures this spatial variability of surface salinity (Figure 4d) across the BoB well, except in the northeastern parts where the model shows lower standard deviation.

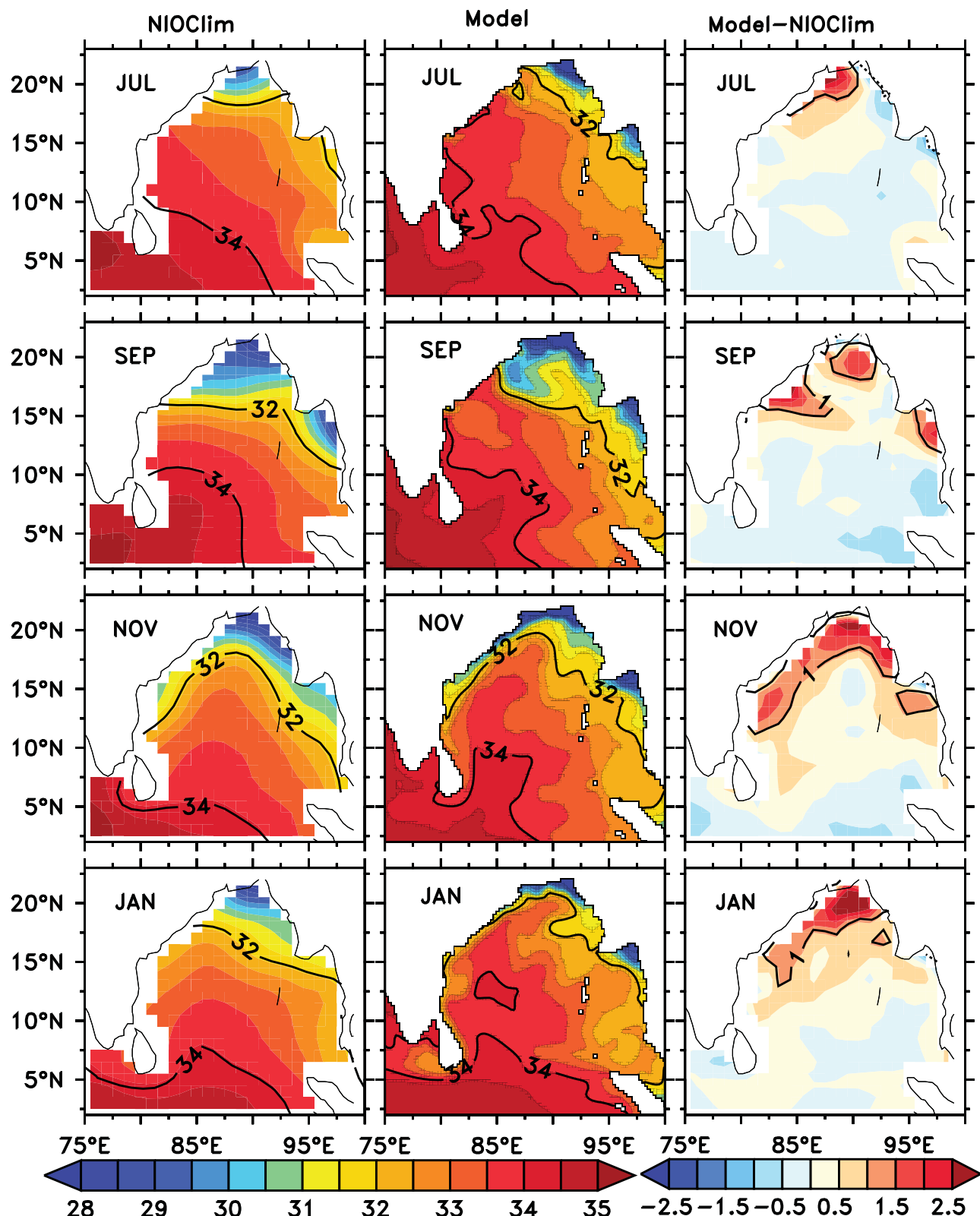


Figure 2. Comparison of SSS of the model (middle plots) with surface salinity of climatology (left plots) obtained from Chatterjee et al. [2012]. Months are chosen based on the signature of freshwater, which is most prominent during summer and winter. SSS difference of 1 psu is contoured in the right plots.

3.2. SST

The model SST from the WRR run is compared with Advanced Microwave Scanning Radiometer-Earth Observing System (AMSR-E) SST climatology. The seasonal cycle of SST in the BoB has a “plateau-like” structure [Vinayachandran and Shetye, 1991] with warming taking place during February–May, a slight cooling with the beginning of the summer monsoon, maintenance of near-steady SST through the summer monsoon and a drastic drop during the winter. This seasonal cycle is well reproduced by the model (Figure 3). The difference between model and AMSR-E climatology is not greater than 0.5°C except in the northwestern BoB during summer (Figure 3) where the model SST is warmer than satellite data. Model SST shows an annual standard deviation of >1°C north of 15°N (Figure 4b), consistent with the AMSR-E climatology. However, standard deviation of annual SST of the model is higher to the south of both India and Sri Lanka. The RMSE of model SST with respect to AMSR-E climatology is <0.5°C in most parts of the bay (Figure 4e) but larger along the southern coasts of India and Sri Lanka, and wherever there is cooling associated with coastal upwelling (not shown), suggesting that the model has a tendency to overestimate coastal upwelling.

3.3. Currents

The basin-scale circulation of the BoB consists of an anticyclonic gyre during January–April [Shetye et al., 1993] and a cyclonic gyre in the southwestern BoB during northeast monsoon (NEM) [Vinayachandran and Yamagata, 1998; Vinayachandran and Mathew, 2003], both of which are well represented by the model (Figure 5). The circulation during summer is dominated by a southeastward Ekman flow in both observation and model [Vinayachandran et al., 2002; Vinayachandran and Kurian, 2007]. The intrusion of the summer monsoon current (SMC) into the bay [Murty et al., 1992; Vinayachandran et al., 1999] and the Sri Lanka Dome [Vinayachandran and Yamagata, 1998] is seen to the east of Sri Lanka.

The EICC has a strong and systematic flow all along the eastern coast of India during the transition periods of monsoon. During February–May, EICC flows poleward as a western boundary current [Legeckis, 1987] of the large seasonal anticyclonic gyre. During November–December, EICC flows equatorward [Shetye et al., 1996] all along the east coast of India, turns around Sri Lanka and transports low salinity water to the south eastern Arabian Sea. During peak summer monsoon, EICC flows equatorward in the northern bay (north of 16°N), poleward in the south bay (between 8°N and 16°N) and southward off the east coast of Sri Lanka. The spatial and temporal variation of western boundary current of the BoB is in good agreement with the observations, as shown in Figure 5. The EICC is associated with several mesoscale eddies along its path [Durand et al., 2009; Mukherjee et al., 2014]. The cyclonic and anticyclonic eddies around Sri Lanka and southeastern coast of India [Vinayachandran and Yamagata, 1998; Durand et al., 2009], respectively, are well reproduced in the model (Figure 5, July). The bifurcation of the EICC during NEM [Vinayachandran et al., 2005] is also captured by the model. During winter, there exists a northward flow in the eastern bay in the model as well as in Ocean Surface Current Analyses Real Time (OSCAR) [Bonjean and Lagerloef, 2002] climatology. (Note that the OSCAR surface current data does not resolve the boundary currents well (Figure 5)). A comparison (Figure 6) of model EICC with OSCAR for three different locations along the east coast of India shows that the model reproduces the observed seasonal cycle. The strength of the poleward flowing EICC is weaker in the model at 18°N. During summer, the equatorial flow north of 18°N reported by Shetye et al. [1991] is confined to the north of 20°N (Figure 5). Thus, the southward flow, seen at 18°N during July–August, is not seen in the model alongshore current. The equatorward current during October–December is captured by the model, with model EICC being stronger. The model alongshore current at 15°N (Figure 6) is almost in phase with the annual cycle of OSCAR current and the current strength are similar during November–December. However, the model current speeds are larger than that of OSCAR surface current during other parts of the year. The model alongshore current at 12°N (Figure 6, black lines) is weaker compared to OSCAR throughout the year. In addition, the model EICC reverses to flow southward earlier by about a month compared to OSCAR. This comparison suggests that the annual cycle of EICC in the model is similar to that in OSCAR, but the model has deficiencies in quantitative comparisons and timing of current reversals.

4. Influence of Freshwater Supply

The contribution of freshwater forcing to the hydrography and circulation of BoB is presented in this section. First, the impact of freshwater on the SSS is presented. Second, freshwater transport within the BoB along its western and eastern boundaries is estimated. The BoB SST response to the freshwater forcing is

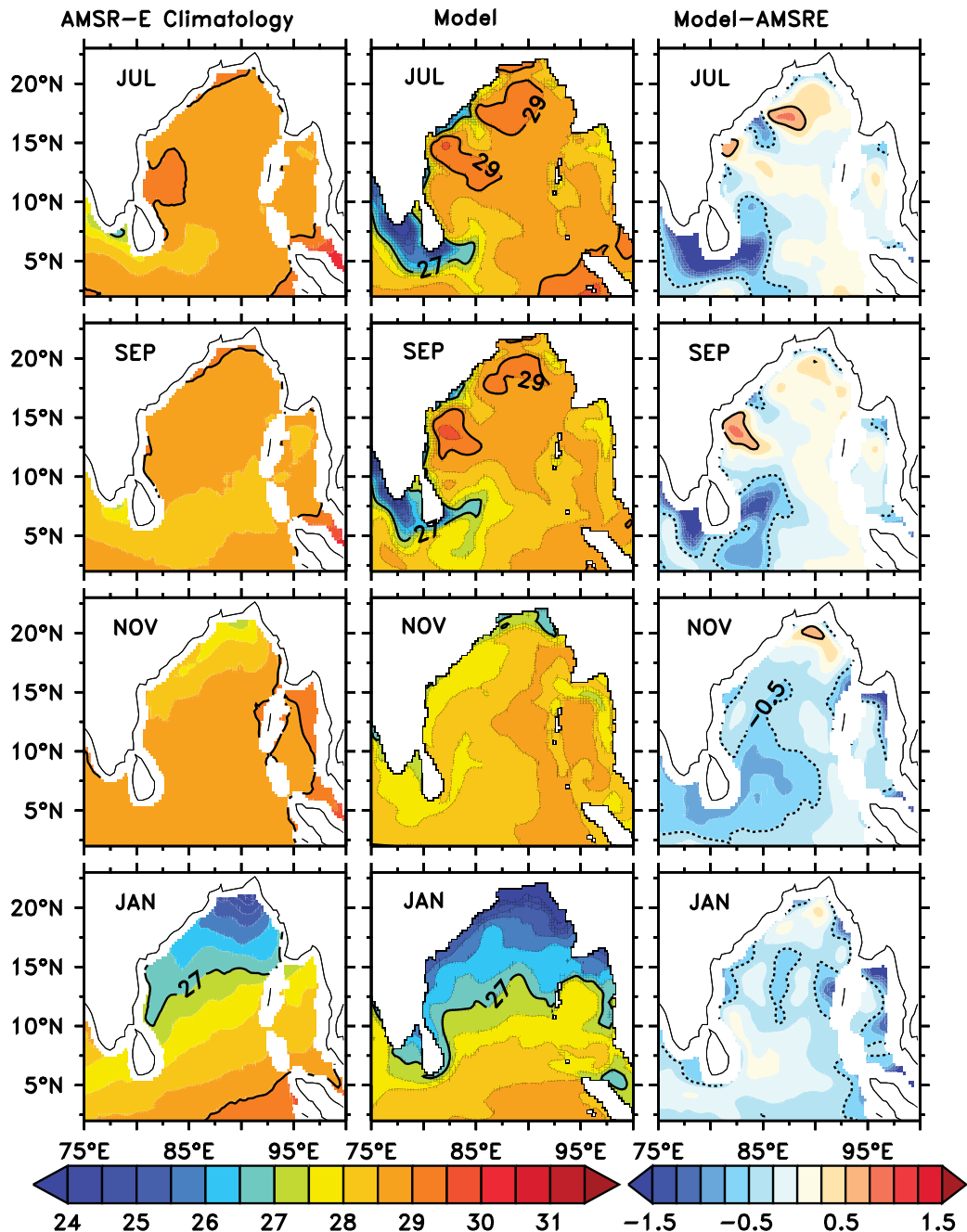


Figure 3. Comparison of model SST (middle plots) at a depth of 2.5 m with SST climatology (left plots) for the period 2003–2008 obtained from AMSR-E. Difference between the two are shown in the right plots. The climatology and the difference plots are spatially smoothed using three point boxcar filter. Contours in the right plots show differences of -0.5°C (dashed lines) and 0.5°C (solid lines). Contours in the left and middle plots show 27°C and 29°C isotherms.

discussed and the processes responsible are evaluated using a heat budget analysis of the MLD. Finally, the impact of freshwater on the formation of temperature inversion is presented.

4.1. SSS

Rainfall and river-runoff encounter the ocean in different ways. Rainfall is spread over a larger area but confined to the surface. River discharge is restricted to the mouths of rivers and affects the upper ocean. The individual and combined effect of rivers and rain on surface salinity is shown in Figure 7. The salinity response to freshwater input is oriented in a southwest-northeast direction with a smaller magnitude toward southwest. WRAIN-NORR (Figure 7, middle) shows that the impact of rainfall is responsible for

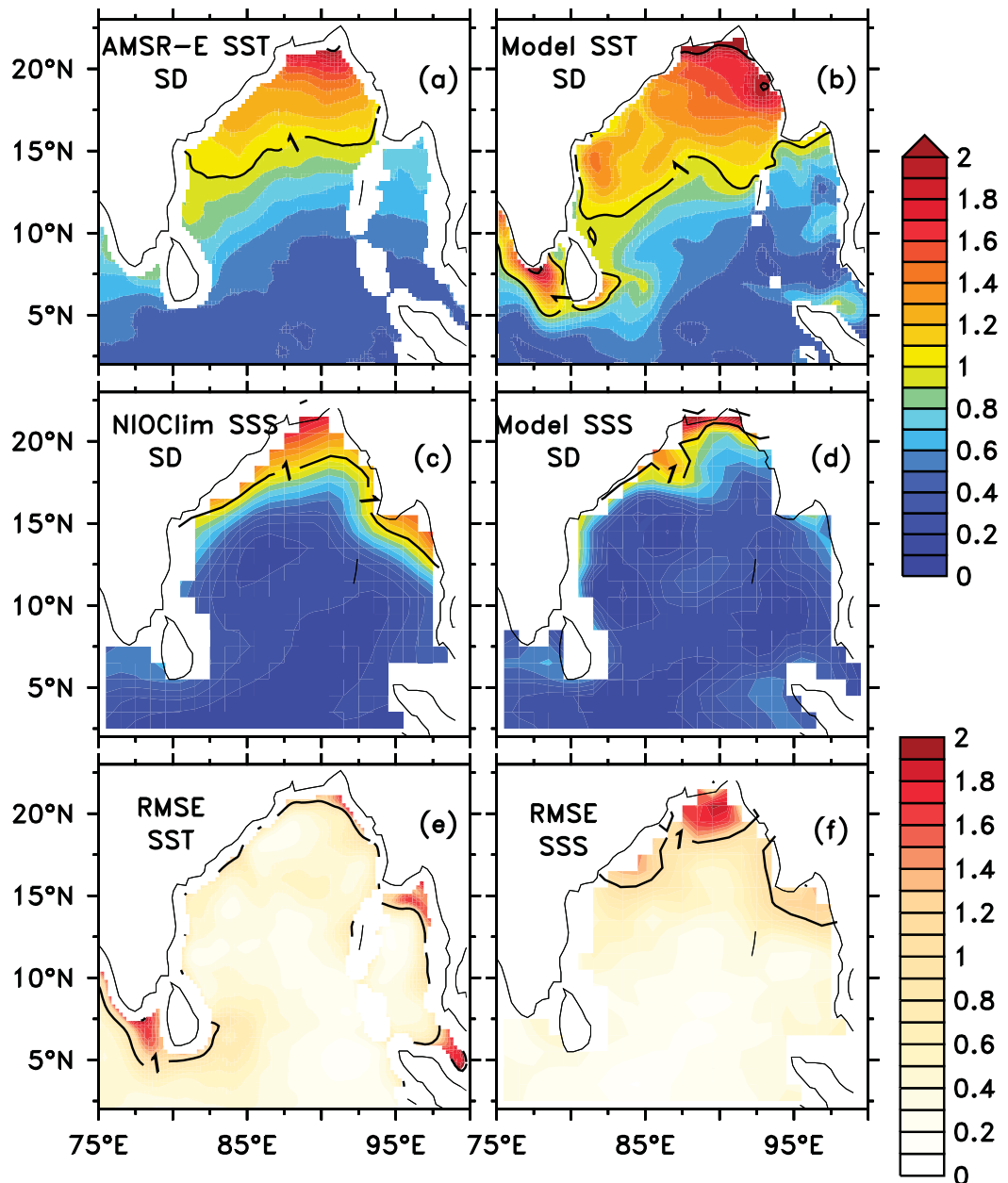


Figure 4. Annual standard deviation of AMSR-E climatology and model SST are shown in the top plots. Annual standard deviation (middle plots) of the model SSS is compared with that of NIOclim. A standard deviation of 1 and 2 is contoured. (bottom) The RMSE of both model SST (left) and SSS (right) with respect to their climatological data sets. RMSE values of 1 and 2 are contoured.

defining this pattern. The river runoff amplifies this signal off the river mouths of Ganges-Brahmaputra (G-B) and along the path of the river plume. Consequently, the highest impact (>2 psu) of combined freshwater forcing is located close to the mouths of G-B toward the end of the summer monsoon (Figure 7). The freshening in the eastern bay is caused by rainfall (Figure 7, middle plots, September), which peaks during the later part of the summer monsoon off the coast of Myanmar. The impact of rain in the eastern bay persists through the NEM (Figure 7). In addition, its effect is also seen along the western boundary during NEM.

After the withdrawal of the SWM, when the EICC flows equatorward, the freshening affects the entire east coast of India and around Sri Lanka (Figure 7, left, November). The combined effect of rain and river is highest during November. The effect of river runoff is seen all along the east coast of India, and this dominates

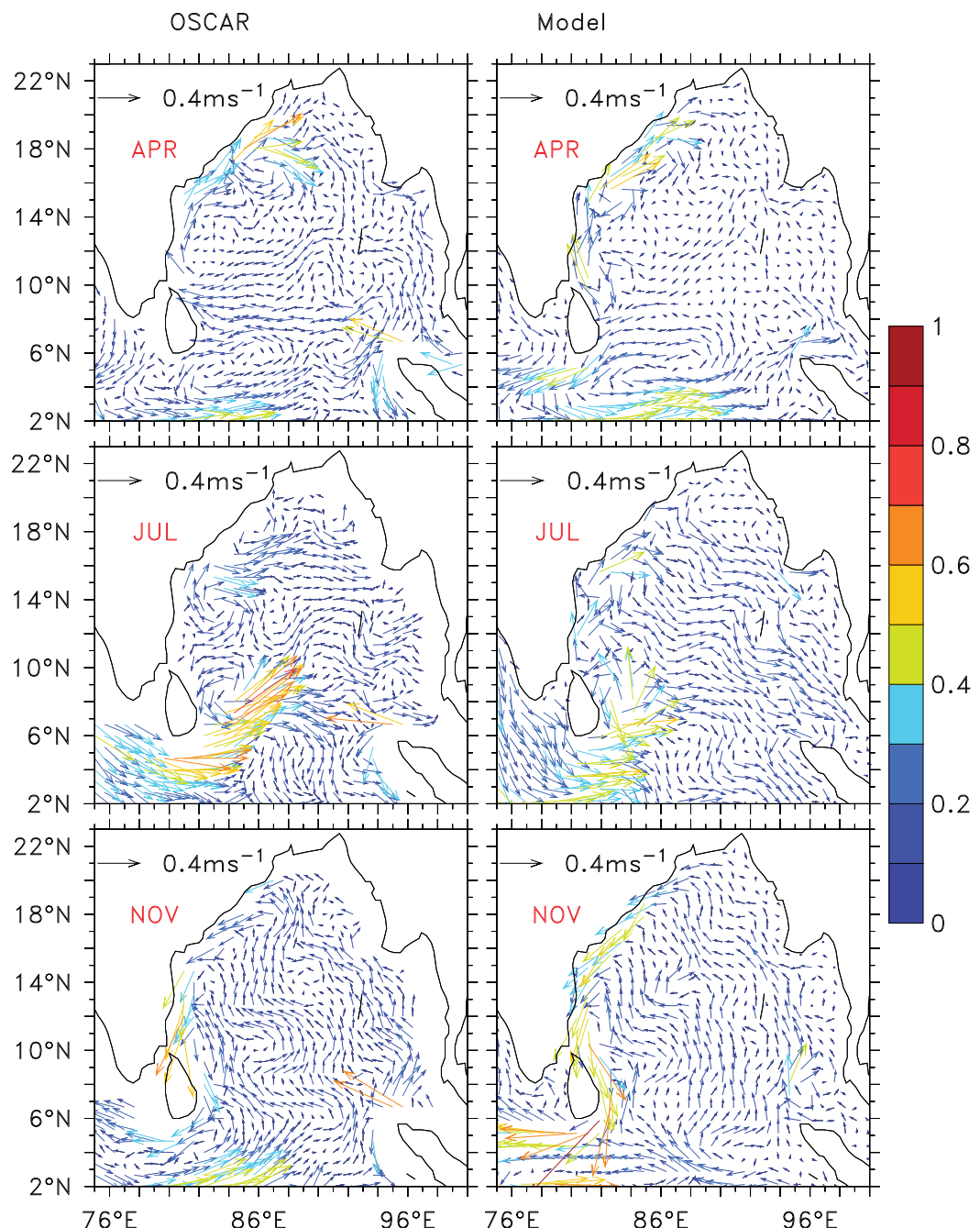


Figure 5. Comparison of model currents (in ms^{-1} , averaged over 30m) with OSCAR climatology. Every third vector is plotted for the model simulation (right) and every second vector for the OSCAR (left). The color of the vectors indicates the current speed.

the impact of rainfall. A southward advection of a low salinity plume made up of both river water and rainfall is also seen during the NEM. As the season advances, larger area of the sea surface is occupied by freshwater, but the southwestern bay is nearly isolated from its influence. In general, model experiments suggest that the open bay is mostly covered with rain water (Figure 7, middle plots, September), which decreases SSS of the bay by 0.5 psu on the western part to >2 psu in the east. Unlike rain water, river water tends to stay closer to coast and results in stronger salinity gradients in the BoB with a salinity decrease of >6 psu near the head bay (Figure 7, right, September). As evident in the first year of the model run, the low salinity plume along the western bay found during the winter mainly comprises of river water.

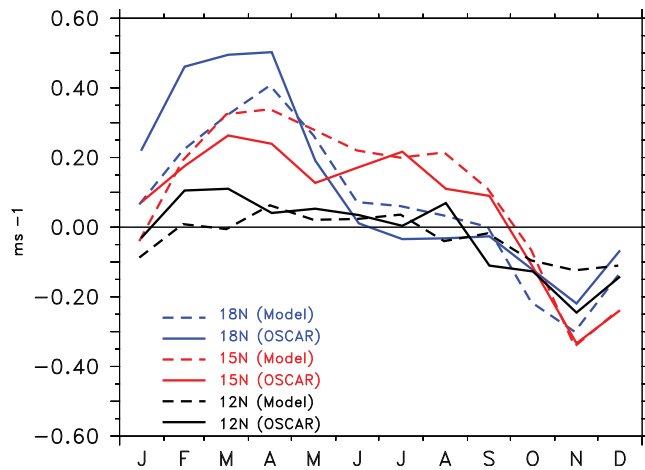


Figure 6. Comparison of alongshore currents (in ms^{-1}) at 12°N , 15°N and 18°N with OSCAR monthly climatology. The model currents are first regressed to the spatial grid of the OSCAR climatology and then averaged across a width of 1.5° offshore.

In addition, the north-south salinity gradient in the bay is maximum during southwest monsoon with surface salinity below 27 psu off the northwestern coast of bay and higher salinity of about 34 psu off the southeastern coast of India during SWM [Shetye et al., 1991]. This strong horizontal gradient of the BoB is intriguing, and suggests the possibility of circulation driven by salinity variations. Han et al. [2001] examined the contribution of river discharge and precipitation on the strength of EICC at a few locations along the east coast of India using a reduced gravity model. Both the contribution of freshwater flux on EICC and its spatial and temporal variations are presented in this section.

The highest impact of freshwater on EICC is seen during early NEM. EICC flows equatorward during November–January (Figures 8a–8c). The rise in the sea level along the east coast of India sets in an equatorward flowing geostrophic current, thereby strengthening the EICC by 0.1 ms^{-1} [Han et al., 2001]. The presence of river forcing (WRIVER) strengthens the equatorward flowing EICC during NEM with an increase in speed by about 0.1 ms^{-1} compared to NORR in the month of November all along the coast (Figure 8). The individual contribution of rainfall forcing to EICC is considerably small ($0.01\text{--}0.03 \text{ ms}^{-1}$). At 20°N , EICC starts flowing southward by August (Figure 8a) and strengthens in the presence of river by $>0.1 \text{ ms}^{-1}$ during October.

4.3. Freshwater Transport

As the BoB receives a large quantity of freshwater on a seasonal time scale, this excess water needs to be transported out of the bay. This is carried out by EICC during November–January [Shetye et al., 1996] on the western side and by equatorward flowing currents in the eastern bay [Han and McCreary, 2001; Jensen, 2001, 2003; Sengupta et al., 2006]. In this section, we examine the contribution of river and rain water to the annual cycle of freshwater transport.

The annual cycle of freshwater transport, T_{fw} calculated based on Schiller et al. [2011] is given by

$$T_{fw} = \int \int F_w V dz dx, \quad (1)$$

where F_w is the fraction of freshwater given by $\frac{S_b - S}{S_b}$ calculated with salinity S from each of the WRR, WRAIN, and WRIVER runs and with a background salinity, S_b , from NORR. The freshwater transport is calculated separately for the western bay and the eastern bay. Along the western boundary, V is the alongshore component of the current. $F_w V$ is integrated across a width of 1.5° (average width of EICC) in the offshore direction and over a depth of 200 m (average depth of EICC) in z direction. Along the eastern boundary, due to the absence of a strong and coastally bounded current, V is taken as the meridional current and $F_w V$ is integrated from 90°E to 99.5°E in x direction over a depth of 100 m [Benshila et al., 2014] along 8°N .

Figures 9a–9c illustrate the annual cycle freshwater transport along the western boundary of the bay at 12°N , 15°N and 18°N . Freshwater is transported southward along the western boundary of the bay during

4.2. Currents

Modeling studies in the past [Potemra et al., 1991; Yu et al., 1991; McCreary et al., 1996; Shankar et al., 1996; Vinayachandran et al., 1996] have established that the EICC is forced by four mechanisms, namely, Ekman pumping in the open bay, remote forcing by winds along the northern and eastern coasts, local winds along the west coast of India and remote forcing from the equatorial Indian Ocean, with remote forcing being more dominant during the transition periods. The influence of freshwater flux on the strength of EICC cannot be ruled out as the shoaling of the ML can trap the momentum within the thin layer, thereby enhancing the current speed.

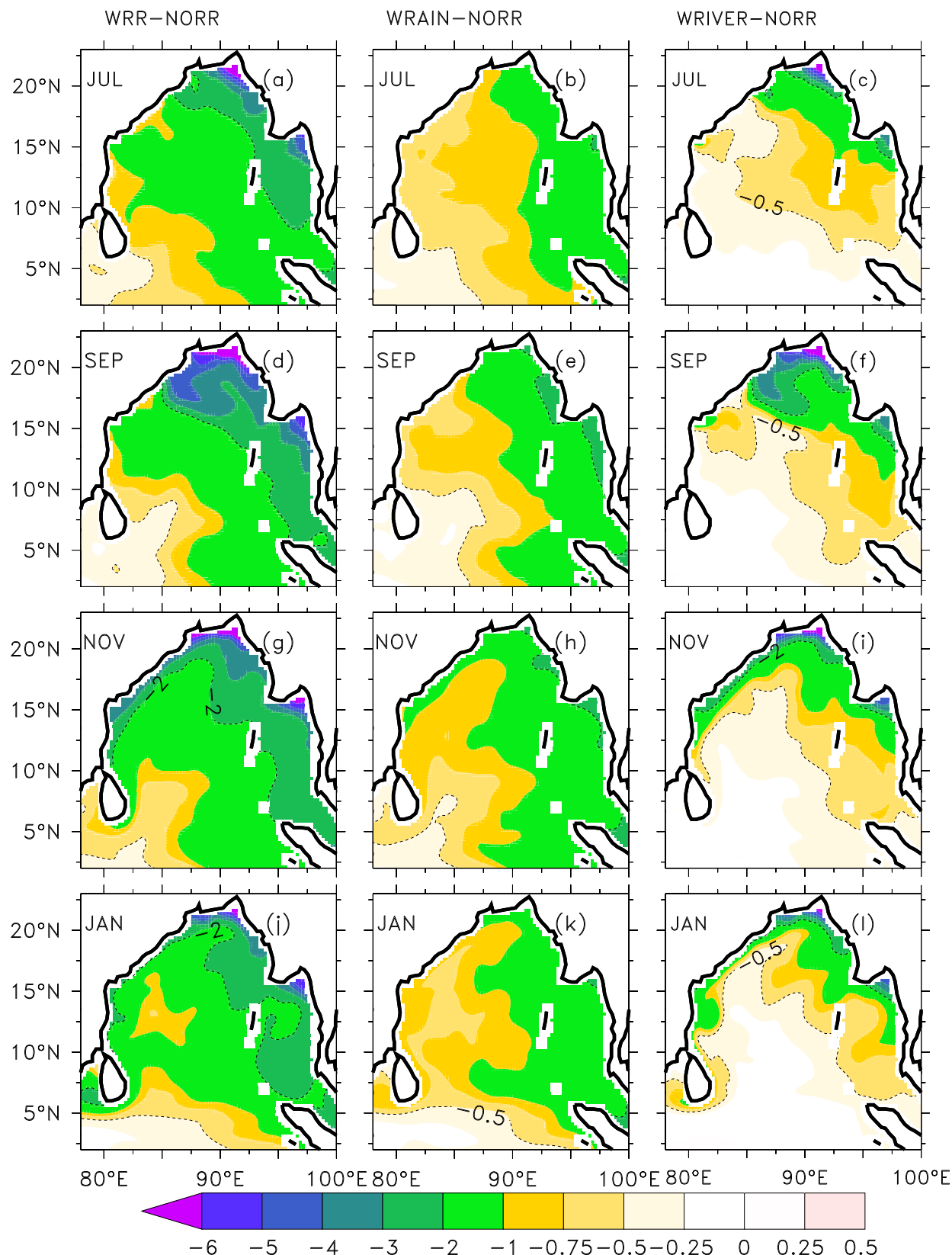


Figure 7. SSS difference between the experiments is shown for the months of July, September, November, and January: (left) WRR-NORR, (middle) WRAIN-NORR, and (right) WRIVER-NORR. Differences of 0.5 psu and 2 psu are contoured.

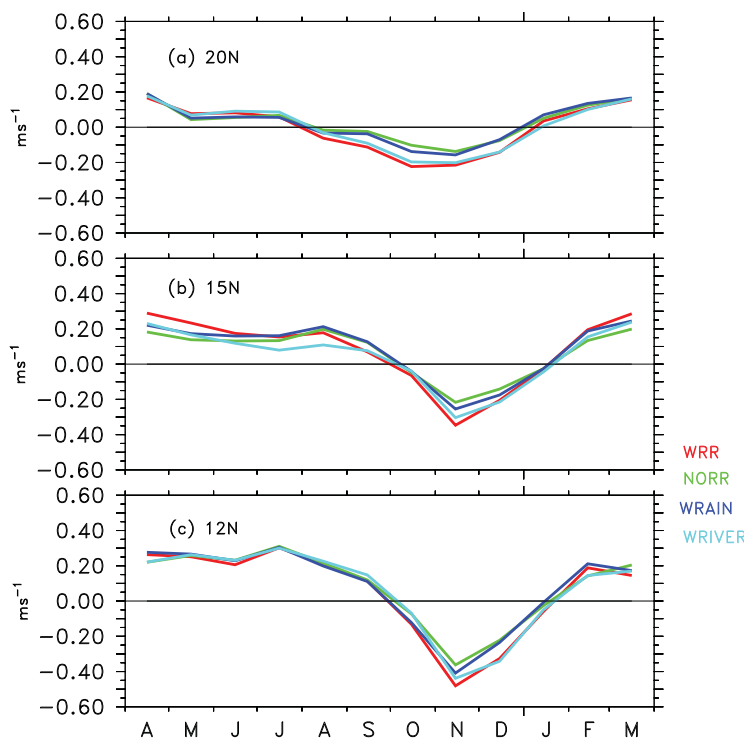


Figure 8. The annual cycle of alongshore component of EICC at (a) 20°N, (b) 15°N, and (c) 12°N for all experiments. The alongshore component of currents at each latitude is averaged across a width of 1.5° starting from the western boundary.

bution of rainfall and river to this low salinity plume. The freshwater transport estimates suggest that a major part of river runoff is advected southward by EICC during November–January.

On the eastern side of the bay, the freshwater is transported southward (Figure 9d) out of the bay at 8°N during both summer and winter with a greater contribution from rainfall. However, there is a northward transport of about 0.15 Sv of freshwater water during November–December. The southward transport of freshwater is maximum during summer (0.3 Sv) and smaller (0.1 Sv) during winter. Figure 9 demonstrates that most of the freshwater flux due to precipitation over the BoB exits along the eastern boundary and that of rivers along the western boundary. This is contrary to the findings of *Benshila et al.* [2014], which emphasizes that the rainwater received by the northern BoB during summer monsoon is exported along the western boundary of the bay. However, *Chaitanya et al.* [2014a] speculates that freshening due to rainfall in the northern bay is during summer and that in southern bay during October–November and summarizes that the low salinity observed along the western boundary is due to river water from far north advected southward post summer monsoon, which is consistent with our study.

4.4. SST

The model experiments show that the SST response to freshwater forcing has considerable spatial preferences that are dependent on the season. The freshwater tends to warm the SST by a maximum of 1.5°C in the northwestern bay during summer monsoon (Figure 10) and is primarily caused by river discharge. In contrast, in the presence of freshwater, the eastern bay is cooler by >1.5°C to a maximum of 3°C adjacent to the coasts throughout the year. SST cooling in the eastern bay spreads offshore and increases with the river input. Rainfall also has the similar impact but with a smaller magnitude of cooling in the eastern part of the BoB (Figure 10).

During NEM, near the head bay, the effect of river runoff is to cool the SST by >2°C, which appears to affect Indian, Bangladesh, and Myanmar coasts. The difference in the signs of SST responses in the western bay and eastern bay (Figure 10) is despite the same SSS response to freshwater (Figure 7). Below we examine in detail the processes controlling the SST changes in different regions.

October–January with a maximum of 0.3 Sv during November at 18°N. Considerable part of this transport is river water amounting to 0.2 Sv and decreases equatorward. In contrast to river water, the southward transport of rainwater along this boundary remains constant from north to south. At 12°N, off the coast of Tamil Nadu which receives rainfall during NEM, T_{fw} is dominated by rainfall. During January–March, EICC flows poleward north of 10°N and T_{fw} is much smaller (not greater than 0.15 Sv) compared to its winter time value. *Akhil et al.* [2014] showed that advection plays a crucial role in the freshening along the western boundary of the BoB during fall and winter. However, their study does not explain the individual contributions of rainfall and river to this low salinity plume. The freshwater transport estimates suggest that a major part of river runoff is advected southward by EICC during November–January.

On the eastern side of the bay, the freshwater is transported southward (Figure 9d) out of the bay at 8°N during both summer and winter with a greater contribution from rainfall. However, there is a northward transport of about 0.15 Sv of freshwater water during November–December. The southward transport of freshwater is maximum during summer (0.3 Sv) and smaller (0.1 Sv) during winter. Figure 9 demonstrates that most of the freshwater flux due to precipitation over the BoB exits along the eastern boundary and that of rivers along the western boundary. This is contrary to the findings of *Benshila et al.* [2014], which emphasizes that the rainwater received by the northern BoB during summer monsoon is exported along the western boundary of the bay. However, *Chaitanya et al.* [2014a] speculates that freshening due to rainfall in the northern bay is during summer and that in southern bay during October–November and summarizes that the low salinity observed along the western boundary is due to river water from far north advected southward post summer monsoon, which is consistent with our study.

4.4. SST

The model experiments show that the SST response to freshwater forcing has considerable spatial preferences that are dependent on the season. The freshwater tends to warm the SST by a maximum of 1.5°C in the northwestern bay during summer monsoon (Figure 10) and is primarily caused by river discharge. In contrast, in the presence of freshwater, the eastern bay is cooler by >1.5°C to a maximum of 3°C adjacent to the coasts throughout the year. SST cooling in the eastern bay spreads offshore and increases with the river input. Rainfall also has the similar impact but with a smaller magnitude of cooling in the eastern part of the BoB (Figure 10).

During NEM, near the head bay, the effect of river runoff is to cool the SST by >2°C, which appears to affect Indian, Bangladesh, and Myanmar coasts. The difference in the signs of SST responses in the western bay and eastern bay (Figure 10) is despite the same SSS response to freshwater (Figure 7). Below we examine in detail the processes controlling the SST changes in different regions.

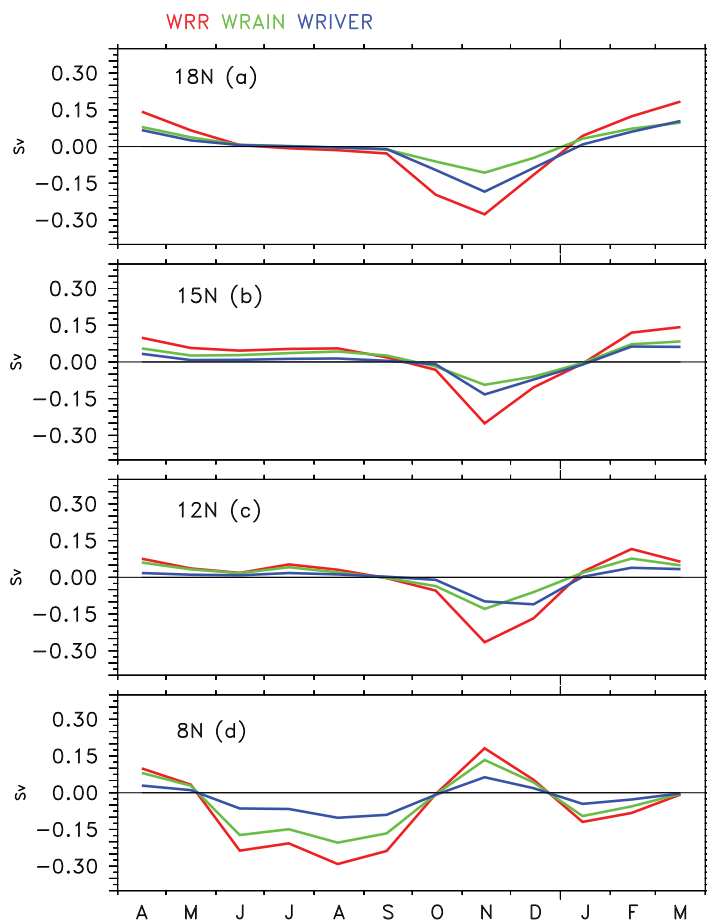


Figure 9. (a), (b), and (c) The annual cycle of alongshore freshwater transport (Sv) along the western boundary in WRR (red), WRAIN (green), and WRIVER (blue) runs at 12°N, 15°N, and 18°N respectively. The alongshore component of EICC is integrated across 1.5° starting from the western boundary of the BoB and over a depth of upper 200 m. (d) The annual cycle of the freshwater transport (Sv) for all the runs near the eastern boundary at 8°N. The meridional component of currents are integrated from 99.5°E to 90°E over a depth of upper 100m.

ency (Figure 11, red line) is given by the sum of Q_{net} and the total shortwave radiation within the ML. Positive (negative) air-sea heat flux term implies heat gain (loss) in the ML. Vertical Processes (Figure 11, purple line) include contribution of vertical mixing and diffusion as parametrized in KPP scheme. The advection term (Figures 11, green line) is the sum of both horizontal and vertical advection. Terms of the equation (2) were saved during the model run and averaged over the MLD that is determined based on the buoyancy criteria defined within the model.

The low salinity patch (Figure 7) in the northern BoB has a smooth gradient with salinity decreasing toward head bay. On the other hand, SST (Figure 10) exhibits different responses at various locations. Considering the different response in the west compared to the east, tendency in the northwestern bay (NWB) to the freshwater forcing is described first followed by the eastern bay. For the NWB, a region bounded by 80°E–89°E and 15°N–20°N is considered. Within this region, for all the grids where the SST difference between WRR and NORR is $>0.25^{\circ}\text{C}$, the ML variables and heat budget terms are averaged. Similarly, for the northeastern bay (NEB) confined between 90°E–96°E and 15°N–22°N, the averaging is done over grids where WRR–NORR SST difference is $<-0.5^{\circ}\text{C}$. These thresholds are chosen based on the differences in SST between the experiments in the respective regions. Response of the ML variables such as salinity, MLD, and temperature is described followed by the annual cycle of heat budget analysis for WRR, NORR, WRAIN, and WRIVER for both summer and winter. Simulations of last 5 years have been compared in order to understand the response of ocean to the freshwater inputs in the absence of atmospheric response to SST

4.4.1. Heat budget of the ML

Temperature equation of the model in the Cartesian form is given by

$$\partial_t(hT) = \underbrace{-\nabla \cdot [h(uT)]}_{\text{horizontal advection}} + \underbrace{\nabla \cdot (hF_h)}_{\text{horizontal mixing}} + \underbrace{(wT)_k - (wT)_{k-1}}_{\text{vertical advection}} + \underbrace{(F_z)_k - (F_z)_{k-1}}_{\text{vertical mixing}}, \quad (2)$$

where T is the temperature of the grid cell of thickness h (in meters), u and w represent the horizontal and vertical current fields, respectively, F_h represents the horizontal subgrid-scale processes, and F_z the vertical mixing. Subscripts k and $k-1$ indicate vertical grids. At the surface, F_z is given by,

$$(F_z)_0 = -\frac{Q_{net}}{\rho C_p}. \quad (3)$$

Here, ρ is the density of the sea water (in kg m^{-3}) and C_p the specific heat of sea water ($\text{J kg}^{-1} \text{C}^{-1}$). Q_{net} is the net air-sea heat flux at the surface, which is the sum of net long-wave radiation, net shortwave radiation, latent heat flux, and the sensible heat flux, and is same for all the experiments. The contribution of air-sea heat flux term (Figure 11, blue line) to the ML temperature tend-

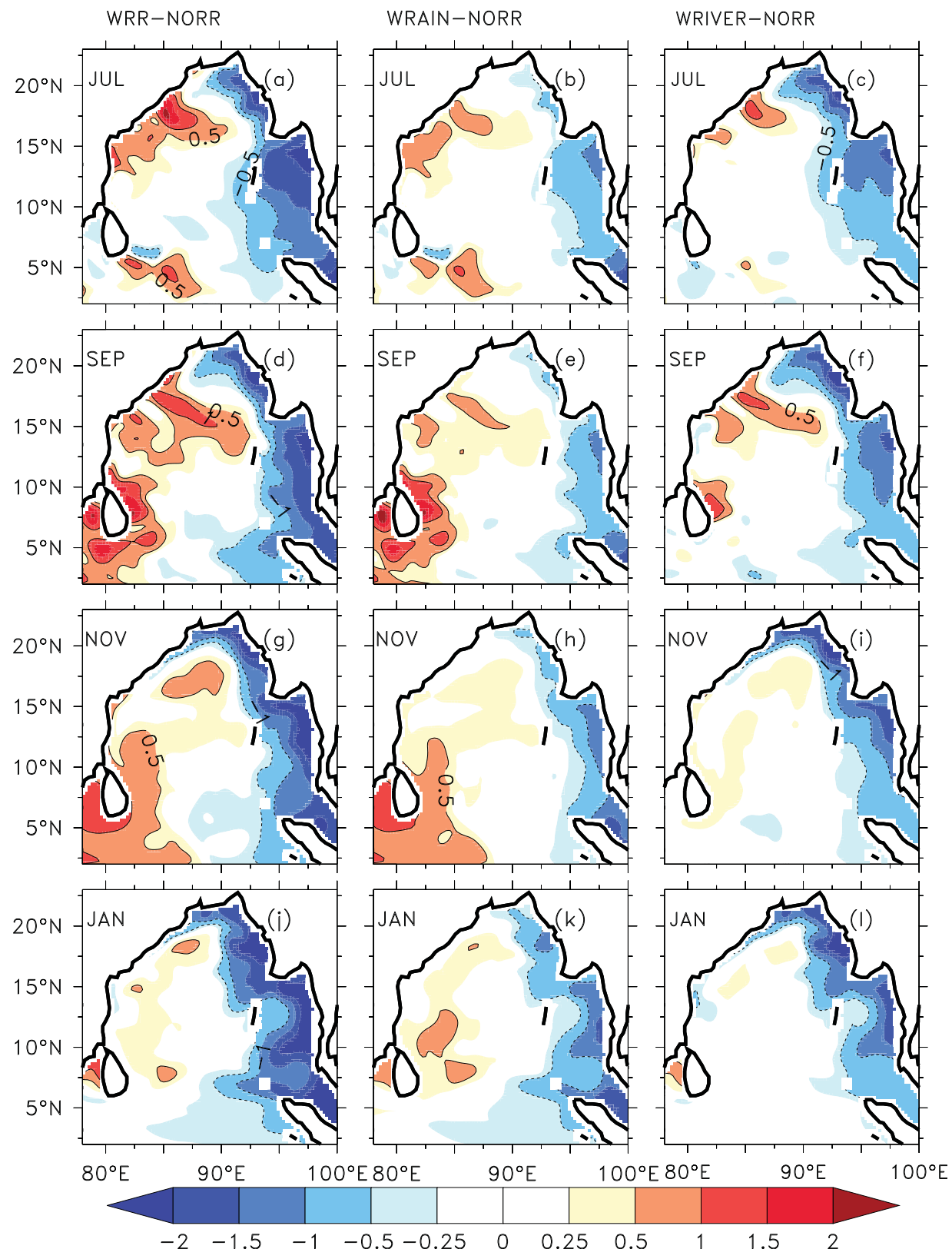


Figure 10. SST difference between the experiments is shown for the months of July, September, November, and January: (left) WRR-NORR, (middle) WRAIN-NORR, and (right) WRIVER-NORR. Solid contours represents SST differences of 0.5°C and 1°C and the dashed contour represent differences of -0.5°C and -1°C .

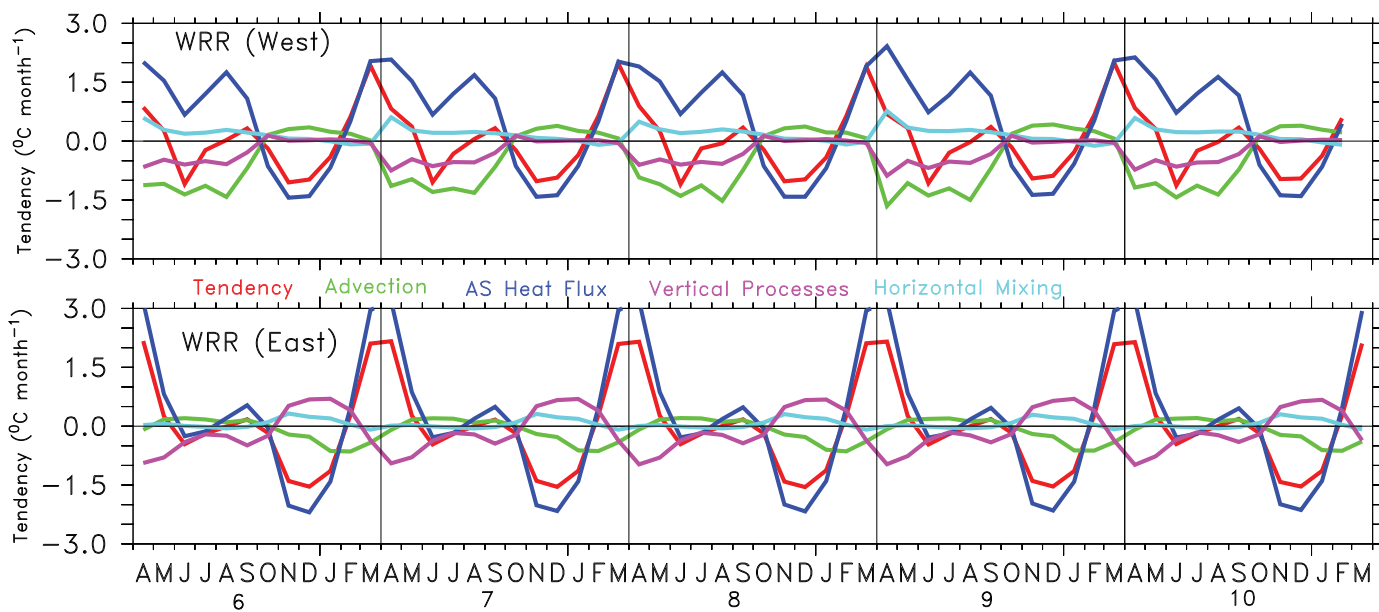


Figure 11. Annual cycles of the ML temperature tendency (red), advection (green), contribution of air-sea heat flux (AS Heat Flux) to the ML temperature tendency (blue), vertical processes (purple), and horizontal mixing (light blue) averaged over the ML in the NWB (top) and NEB (bottom). Last 5 year results of WRR are shown.

changes. In the NWB (Figure 11, top), the annual cycle of terms contributing to temperature tendency in WRR highlights the role of air-sea heat flux term. However, advection and vertical processes cause cooling during the SWM, which reduces the impact of heat gain substantially. In NEB (Figure 11, bottom), heat gain within the ML dominates the tendency and it may be noted that vertical processes have a warming tendency during winter.

4.4.1.1. Northwestern Bay

In the presence of freshwater input, the surface salinity lowers by about 2.5 psu toward the end of the SWM (Figure 12a). The MLD shoals by about 10 m during SWM and about 30 m during NEM. The temperature is warmer by about 1°C during SWM and 0.5°C during NEM. The river and rain water is found to have roughly equal individual contribution toward these differences. The river runoff leads to greater loss of shortwave below the ML compared to rainwater, and this process is significant during the SWM. Air-sea interaction influences the mixed layer temperature in two ways. First, a shallow MLD implies greater SST increase compared to a deeper ML for the same amount of net heat gain from the atmosphere. Second, a shallow ML can also result in greater penetrative shortwave heat loss compared to a thick ML (Figure 12a). The heating or cooling due to the air-sea heat flux term depends on the mean MLD during a particular season and the changes in the MLD owing to the freshwater inputs. The net result in the NWB is that the warming tendency due to air-sea heat flux term is greater in the presence of freshwater input during SWM owing to heat gain within the shallow MLD, and lower during post monsoon (Figure 12b) owing to the greater shortwave loss below the MLD. Stratification due to river discharge has a greater influence on this air-sea heat flux term. In summary, the warming during SWM (Figure 10) in the presence of freshwater input appears to be primarily due to distribution of the air-sea heat flux over a thinner ML during summer.

During winter, the contribution of air-sea heat flux is negative (Figure 11, top) and lowers the temperature. This cooling is maximum in the presence of freshwater input owing to its thin MLD. In contrast, vertical processes (Figure 12b) contribute to the warming owing to the strong stratification. The circulation of western bay is distinct with the presence of strong and narrow coastally trapped western boundary current. During spring, advection plays a crucial role in cooling the SST (Figures 11, top), however, to a lesser extent in the presence of freshwater. The net effect of advection is to warm the NWB during spring. This analysis suggests that all processes contributing to the temperature tendency are modified when there is freshwater input.

4.4.1.2. Northeastern Bay

The SSS, in the presence of freshwater input, lowers by about 5 psu during the peak summer (Figure 13a). The MLD shoals by 15 m during both summer and winter. Substantial SST response to the freshwater input

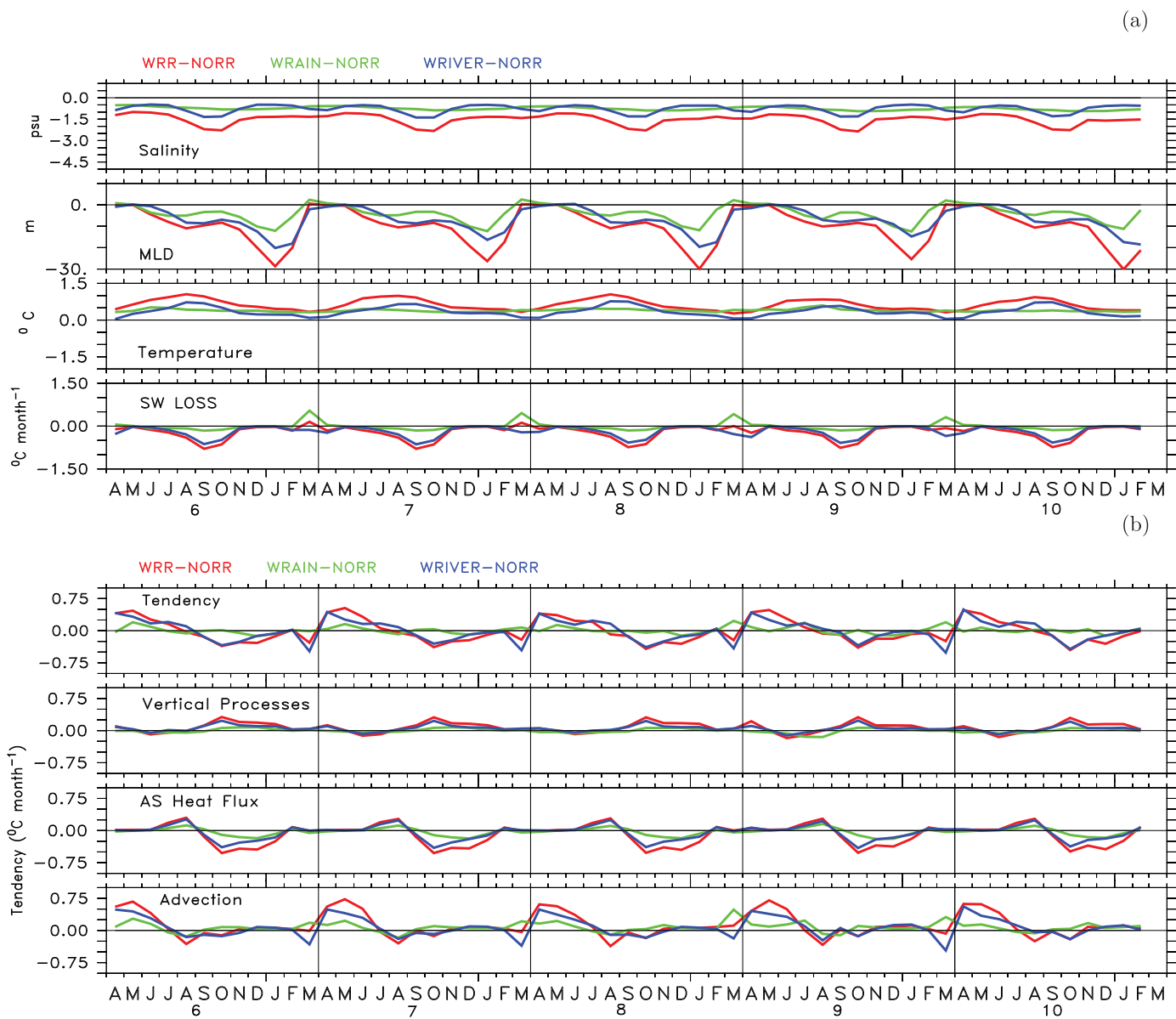


Figure 12. Annual cycles of the changes in (a) MLD, ML temperature, ML salinity, and shortwave loss below the ML and (b) heat budget terms (refer to Figure 11) averaged over the ML in the NWB. Last 5 year results of the changes due to rainfall (WRain-NORR, green), river discharge (WRIVER-NORR, blue), and both the freshwater inputs (WRR-NORR, red) are shown.

with a major contribution from river discharge into the eastern BoB is seen only during NEM, which is then preserved (Figure 13a). Advection slightly warms the SST during spring and summer. However, during summer, the ML is shallower in the presence of freshwater, and consequently shortwave absorption is less (Figures 13a and 13b). Owing to these opposing processes, the net effect is that there is small difference in tendency between experiments (Figure 13b).

During NEM, in the presence of freshwater, the MLD is thinner (Figure 13a) and consequently for the same air-sea heat loss, the air-sea heat flux tendency term has a larger contribution to the temperature tendency (Figure 13b) compared to when the freshwater is absent. Advection has a cooling tendency in this region (Figures 11, bottom). In the presence of freshwater input, advection slightly cools the SST, while the vertical processes warms the SST owing to the strong salinity stratification. Net cooling of the SST during a particular year is not compensated in the following season and the SST cools further during the following winter. Thus, the air-sea heat loss during winter has a major contribution in cooling the SST when freshwater supply is present in the NEB (Figure 13a). This is in contrast to the west where processes in winter try to rectify the

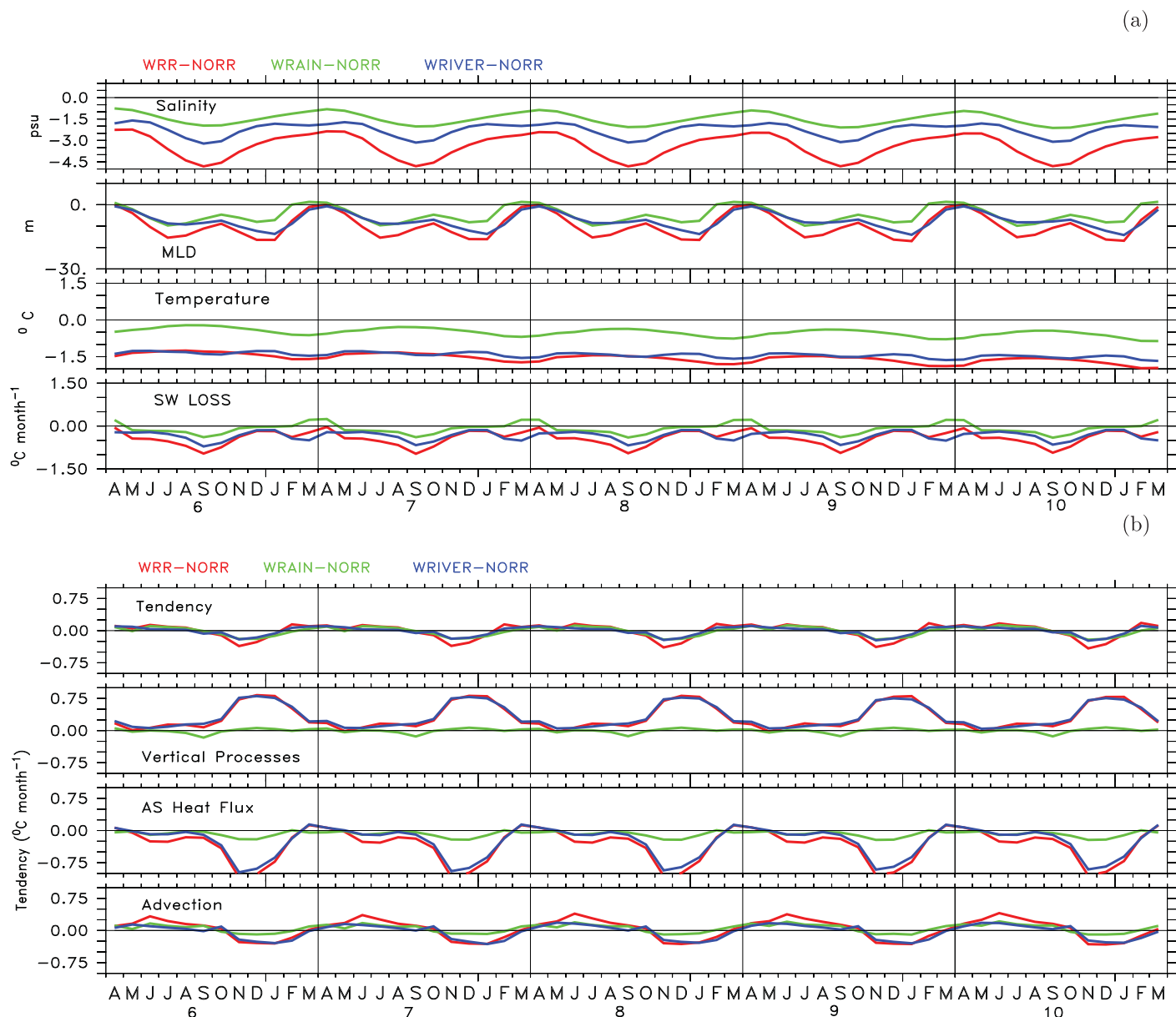


Figure 13. Same as in Figure 12 but for the NEB.

SST response during spring and summer. Consequently, the NEB presents larger response to freshwater input compared to the NWB.

5. Temperatures Inversion

Thin ML commonly occurring in the BoB is highly favorable for the formation of TI. Presence of TI has been reported from the BoB by observations during both summer [Shetye et al., 1996; Vinayachandran et al., 2002] and winter [Shetye et al., 1996; Thadathil et al., 2002; Girishkumar et al., 2013]. TI can warm a deepening ML as the water that is entrained to the ML is warmer [Smyth et al., 1996; Kurian and Vinayachandran, 2006; de Boyer Montégut et al., 2007]. Several processes can lead to the formation of TI, but salinity stratification is an essential prerequisite. Cooling of a thin ML can lead to TI formation and advection of cooler low salinity water above a warmer layer can also lead to TI when the ML is shallow. Shortwave radiation penetrating beneath the ML can cause TI, provided that the ML heat gain is less than the warming beneath.

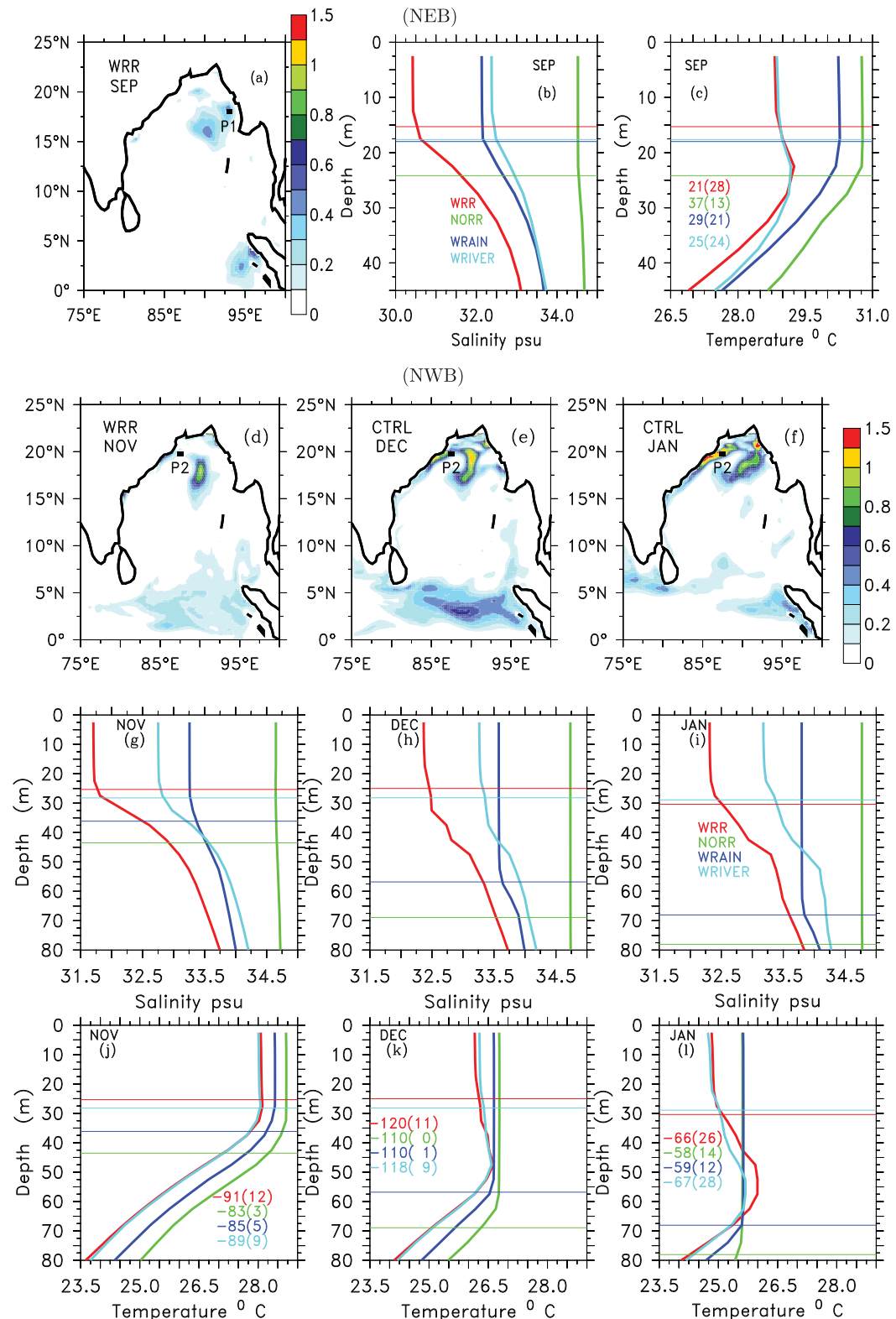


Figure 14. Spatial distribution of TI for summer (September) at a location P1 (marked in (a)) in the NEB (a–c) and for winter (November–January) at a location P2 (marked in (d)) in the NWB (d–l). Vertical profiles of salinity and temperature corresponding to locations P1 and P2 are shown for WRR (red), NORR (green), WRRAIN (blue), and WRIVER (light blue). Horizontal lines represent the MLD for each experiment. Numbers represent heat gain/loss in the ML and the numbers within the brackets indicate shortwave radiation lost below the ML.

TI in the BoB are found both during summer and winter in the model simulation (Figure 14), but not during March–April. The existence of TI in the western bay during summer has been reported by *Shetye et al.* [1996] and *Thadathil et al.* [2002]. During summer, the northeastern part of the bay has a TI of $>0.25^{\circ}\text{C}$ (significant TI based on *Shankar et al.* [2004]). At P1, a location in the NEB (Figure 14a), the salinity profile (Figure 14b) shows a drop in SSS by 4 psu in WRR due to freshwater forcing. The thin MLD present in WRR, WRRAIN, and WRIVER runs show the impact of vertical stratification induced by either of the freshening sources. A TI of about 0.5°C occurs in WRR at around 25 m below the surface, about 0.3°C is seen in WRIVER, and a much smaller magnitude of $<0.2^{\circ}\text{C}$ in WRRAIN (Figure 14c). In the presence of freshwater forcing, the shortwave penetrative loss of about 28 Wm^{-2} below the thin ML is responsible for the formation of TI. In NORR, absence of the barrier layer ensures greater shortwave heat absorption within the MLD. However, despite the same MLD in WRIVER and WRRAIN, the TI is found to be contributed by the advection of cooler river water at the surface, which results in cooling the SST by about 2°C . Therefore, Figures 14a–14c show that river water contributes to the formation of TI in the NEB by heating up the layer below the MLD and the horizontal advection of cooler river water at the surface.

The existence of TI in the western bay during summer has been reported by *Shetye et al.* [1996] and *Thadathil et al.* [2002]. However, TI in the western bay is found to be maximum during winter. Western bay has inversions hugging all along the east coast of India (Figures 14d–14f) in the model, with a maximum TI close to the land boundaries. Figures 14g–14i show the salinity profiles of different experiments at a location, P2, in the western bay for the months of November, December, and January. Freshening causes the surface salinity to drop by about 1–2 psu in WRR during November–January. The MLD is not very different between these months in WRR and WRIVER; however, in NORR and WRRAIN, weaker stratification and wind-mixing result in a deeper MLD during December–January. A barrier layer of thickness of about 45 m is also found in WRR, but absent in NORR and WRRAIN. The Northern BoB experiences a decrease in SST due to latent heat loss within a thin MLD during winter. The bay exhibits substantial surface cooling of about 2°C from November to December (Figure 14k). In WRR and WRIVER, confinement of the cooling within the shallow MLD results in TI at this location. Surface is further cooled by 1.5°C in WRIVER and WRR from December to January. A maximum TI of about 1.1°C is found at depth of around 60 m during January (Figure 14l) in WRR and about 1°C in WRIVER located within the barrier layer. Relatively smaller magnitudes of shortwave penetrative loss at the base of the MLD suggest that the subsurface inversions are primarily caused by the surface cooling during winter. Absence of TI in NORR and WRRAIN signify the role of strong vertical stratification induced due to the freshening by river water in the western bay.

6. Summary and Conclusions

The capacity of the BoB to remain warm through the summer has been attributed to the freshwater that it receives from rainfall and river runoff. Earlier modeling studies have suggested that the warming during summer owing to freshwater effects is rather small. In this study, we carried out a set of numerical experiments using an OGCM to separate the effects of river discharge and rainfall on SSS, SST, currents, freshwater export, and TI. These experiments retain either river or rain or both, and the differences between them and the experiment without freshwater inputs are considered to give the impact of retained freshwater component. All the sensitivity experiments were carried out for 10 years. The air-sea heat flux is maintained to be the same in all experiments. These numerical experiments have been able to separate the spatiotemporal pattern of the influence of rainfall and river runoff on the SST, SSS, and currents.

The runoff, besides from causing low salinity near the mouths of rivers, affects the northwestern bay during summer monsoon. A tongue of low salinity extends offshore in the northwestern bay comprises of river water. During NEM, effect of rivers is restricted to the east coast of India. Rainfall, on the other hand, has a much larger areal spread but causes smaller decrease in salinity, and has larger impact in the eastern half of the bay compared to the west. The equatorward flowing EICC during NEM is strengthened by about 0.15 ms^{-1} due to the river forcing. The EICC during summer also shows an increase in strength of the freshwater plume at 20°N due to the runoff. The freshwater transport estimates suggests that major part of river water is carried by southward flowing EICC during NEM. Despite the absence of strong currents, the meridional freshwater transport at 8°N highlights the export of rain water out of the bay along the eastern boundary of the BoB.

Mixed layer variables and terms of the model temperature equation have been examined to investigate processes that are responsible for the SST difference between experiments. Strong salinity stratification warms the sea surface in the NWB and the warm regions spread offshore. This warming is found to be maximum ($\sim 1.5^{\circ}\text{C}$) near the river mouths during SWM; the warming tendency is attributed to reduced vertical mixing and net heat gain within the shallow ML in the presence of freshwater, with a greater contribution from rain during the early SWM, followed by that from river discharge for the rest of the season. In NEB, in the presence of freshwater, despite reduced vertical mixing and temperature inversions below the MLD, the net heat loss over a shallow MLD aided with horizontal advection results in substantial cooling during NEM. The contribution of river discharge to cooling is maximum during winter. Owing to the lack of compensating processes, during the rest of the year, the winter cooling is retained.

A location representing western bay exhibits a TI of about 1.1°C during January. Temperature and salinity profiles during winter shows that the TI in the western bay are caused due to air-sea heat losses within a shallow MLD. The TI is present only in WRR and WRIVER signifies the contribution of river water in the northwestern bay. During summer, only eastern bay exhibits TI. Eastern bay shows a TI of about 0.5°C , owing to the forcing of both river and rain. Heat absorbed within the thin ML is lowest in WRR compared to other experiments, and the shortwave radiation at the base of the ML determines the role of heating the barrier layer by the penetrative shortwave radiation in the presence of strong stratification leading to TI formation.

In summary, by prescribing the same air-sea heat flux in all the experiments, it is demonstrated that the NWB remains warmer by $>1^{\circ}\text{C}$ during the SWM owing to the strong salinity stratification, though NEB has a substantial cooling tendency in the winter, which is preserved over the subsequent seasons. To conclude, freshwater input enhances the impact of warming in the NWB and cooling in the NEB. These results suggest that accurate regional SST forecast in the BoB would require accurate estimates of each component of the freshwater input and their spatiotemporal patterns.

Acknowledgments

This study was funded by the Indian Ocean Modeling (HOOFS) programme of Indian National Center for Oceanic Information Services (INCOIS), Hyderabad. NCEP Reanalysis data was provided by the NOAA/OAR/ESRL PSD, Boulder, Colorado, USA (www.esrl.noaa.gov/psd/). QuikSCAT by Remote Sensing Systems and sponsored by the NASA Ocean Vector Winds Science Team (www.remss.com). We also acknowledge SeaWiFS mission scientists and associated NASA personnel for the production of the data used in this research effort. Computations were carried out on a high performance computer (HPC) system facility at CAOS, IISc, funded by Department of Science and Technology under Fund for Improvement of S&T Infrastructure in Universities and Higher Educational Institutions (FIST) scheme and Divecha Center for Climate Change (DCCC). We thank GFDL for providing the MOM4p1 source code. We thank two anonymous reviewers whose careful reading and thorough reviews helped us to improve the clarity of the paper.

References

- Akhil, V., F. Durand, M. Lengaigne, J. Vialard, M. Keerthi, V. Gopalakrishna, C. Deltel, F. Papa, and C. de Boyer Montégut (2014), A modeling study of the processes of surface salinity seasonal cycle in the Bay of Bengal, *J. Geophys. Res. Oceans*, **119**, 3926–3947, doi:10.1002/2013JC009632.
- Antonov, J. I., D. Seidov, T. P. Boyer, R. A. Locarnini, A. V. Mishonov, H. E. Garcia, O. K. Baranova, M. M. Zweng, and D. R. Johnson (2010), *World Ocean Atlas 2009 Volume 2: Salinity*, vol. 2, 184 pp., U.S. Gov. Print. Off., Washington, D.C.
- Benshila, R., F. Durand, S. Masson, R. Bourdallé-Badie, C. de Boyer Montégut, F. Papa, and G. Madec (2014), The upper Bay of Bengal salinity structure in a high-resolution model, *Ocean Model.*, **74**, 36–52.
- Bonjean, F., and G. S. Lagerloef (2002), Diagnostic model and analysis of the surface currents in the tropical Pacific Ocean, *J. Phys. Oceanogr.*, **32**(10), 2938–2954.
- Chaitanya, A., M. Lengaigne, J. Vialard, V. Gopalakrishna, F. Durand, C. Kranthikumar, S. Amritash, V. Suneel, F. Papa, and M. Ravichandran (2014a), Salinity measurements collected by fishermen reveal a river in the sea flowing along the eastern coast of India, *Bull. Am. Meteorol. Soc.*, **95**(12), 1897–1908.
- Chaitanya, A. V. S., F. Durand, S. Mathew, V. V. Gopalakrishna, F. Papa, M. Lengaigne, J. Vialard, C. Kranthikumar, and R. Venkatesan (2014b), Observed year-to-year sea surface salinity variability in the Bay of Bengal during the 2009–2014 period, *Ocean Dyn.*, **65**(2), 173–186.
- Chassignet, E. P., and Z. D. Garraffo (2001), Viscosity parameterization and the Gulf Stream separation, in *From Stirring to Mixing in a Stratified Ocean, Proceedings of Hawaiian Winter Workshop, January 16–19, 2001*, edited by P. Muller and D. Henderson, pp. 37–41, Univ. of Hawaii at Manoa, Honolulu.
- Chatterjee, A., D. Shankar, S. S. C. Shenoi, G. V. Reddy, G. S. Michael, M. Ravichandran, V. V. Gopalakrishna, E. P. R. Rao, T. V. S. U. Bhaskar, and V. N. Sanjeevan (2012), A new atlas of temperature and salinity for the North Indian Ocean, *J. Earth Syst. Sci.*, **121**, 559–593, doi:10.1007/s12040-012-0191-9.
- Dai, A., and K. E. Trenberth (2002), Estimates of freshwater discharge from continents: Latitudinal and seasonal variations, *J. Hydrometeorol.*, **3**(6), 660–687.
- de Boyer Montégut, C., J. Mignot, A. Lazar, and S. Cravatte (2007), Control of salinity on the mixed layer depth in the world ocean: 1. General description, *J. Geophys. Res.*, **112**, C10010, doi:10.1029/2006JC003954.
- Durand, F., D. Shankar, C. de Boyer Montégut, S. S. C. Shenoi, B. Blanke, and G. Madec (2007), Modeling the barrier-layer formation in the Southeastern Arabian Sea*, *J. Clim.*, **20**(10), 2109–2120.
- Durand, F., D. Shankar, F. Birol, and S. S. C. Shenoi (2009), Spatiotemporal structure of the East India Coastal Current from satellite altimetry, *J. Geophys. Res.*, **114**, C02013, doi:10.1029/2008JC004807.
- Egbert, G. D., and S. Y. Erofeeva (2002), Efficient inverse modeling of barotropic ocean tides, *J. Atmos. Oceanic Technol.*, **19**(2), 183–204.
- Egbert, G. D., A. F. Bennett, and M. G. G. Foreman (1994), TOPEX/POSEIDON tides estimated using a global inverse model, *J. Geophys. Res.*, **99**(C12), 24,821–24,852.
- Fekete, B., C. Vörösmarty, and W. Grabs (2002), Global composite runoff fields on observed river discharge and simulated water balances/ Water System Analysis Group, technical report no. 22, Univ. of N. H., and Global Runoff Data Cent., Fed. Inst. of Hydrol. (BfG), Koblenz, Germany.
- Fox-Kemper, B., and R. Ferrari (2008), Parameterization of mixed layer eddies. Part II: Prognosis and impact, *J. Phys. Oceanogr.*, **38**(6), 1166–1179.

- Fox-Kemper, B., G. Danabasoglu, R. Ferrari, and R. Hallberg (2008), Parameterizing submesoscale physics in global models, *Climat Exchanges*, 13, 3–5.
- Girishkumar, M. S., M. Ravichandran, M. McPhaden, and R. Rao (2011), Intraseasonal variability in barrier layer thickness in the south central Bay of Bengal, *J. Geophys. Res.*, 116, C03009, doi:10.1029/2010JC006657.
- Girishkumar, M. S., M. Ravichandran, and M. J. McPhaden (2013), Temperature inversions and their influence on the mixed layer heat budget during the winters of 2006–2007 and 2007–2008 in the Bay of Bengal, *J. Geophys. Res. Oceans*, 118, 2426–2437, doi:10.1002/jgrc.20192, 2013.
- Griffies, S. M. (1998), The Gent-McWilliams skew flux, *J. Phys. Oceanogr.*, 28(5), 831–841.
- Griffies, S. M., A. Gnanadesikan, R. C. Pacanowski, V. D. Larichev, J. K. Dukowicz, and R. D. Smith (1998), Isoneutral diffusion in a z-coordinate ocean model, *J. Phys. Oceanogr.*, 28(5), 805–830.
- Griffies, S. M., M. Schmidt, and M. Hereld (2009), Elements of MOM4p1, *GFDL Ocean Group Tech. Rep.*, 6, 444 pp., NOAA/Geophysical Fluid Dynamics Laboratory, Princeton, N. J.
- Han, W., and J. P. McCreary (2001), Modeling salinity distributions in the Indian Ocean, *J. Geophys. Res.*, 106(C1), 859–877.
- Han, W., J. P. McCreary, and K. E. Kohler (2001), Influence of precipitation minus evaporation and Bay of Bengal rivers on dynamics, thermodynamics, and mixed layer physics in the upper Indian Ocean, *J. Geophys. Res.*, 106(C4), 6895–6916.
- Howden, S. D., and R. Murtugudde (2001), Effects of river inputs into the Bay of Bengal, *J. Geophys. Res.*, 106(C9), 19,825–19,843.
- Jackett, D. R., T. J. McDougall, R. Feistel, D. G. Wright, and S. M. Griffies (2006), Algorithms for density, potential temperature, conservative temperature, and the freezing temperature of seawater, *J. Atmos. Oceanic Technol.*, 23(12), 1709–1728.
- Jensen, T. G. (2001), Arabian Sea and Bay of Bengal exchange of salt and tracers in an ocean model, *Geophys. Res. Lett.*, 28(20), 3967–3970.
- Jensen, T. G. (2003), Cross-equatorial pathways of salt and tracers from the northern Indian Ocean: Modelling results, *Deep Sea Res., Part II*, 50(12), 2111–2127.
- Kalnay, E., et al. (1996), The NCEP/NCAR 40-year reanalysis project *Bull. Am. Meteorol. Soc.*, 77(3), 437–471.
- Kurian, J., and P. Vinayachandran (2006), Formation mechanisms of temperature inversions in the southeastern Arabian Sea, *Geophys. Res. Lett.*, 33, L17611, doi:10.1029/2006GL027280.
- Kurian, J., and P. N. Vinayachandran (2007), Mechanisms of formation of the Arabian Sea mini warm pool in a high-resolution Ocean General Circulation Model, *J. Geophys. Res.*, 112, C05009, doi:10.1029/2006JC003631.
- Large, W. G., and S. G. Yeager (2004), *Diurnal to Decadal Global Forcing for Ocean and Sea-Ice Models: The Data Sets and Flux Climatologies*, Natl. Cent. for Atmos. Res., Boulder, Colo.
- Large, W. G., J. C. McWilliams, and S. C. Doney (1994), Oceanic vertical mixing: A review and a model with a nonlocal boundary layer parameterization, *Rev. Geophys.*, 32(4), 363–403.
- Lee, H.-C., A. Rosati, and M. J. Spelman (2006), Barotropic tidal mixing effects in a coupled climate model: Oceanic conditions in the Northern Atlantic, *Ocean Modell.*, 11(3), 464–477.
- Legeckis, R. (1987), Satellite observations of a western boundary current in the Bay of Bengal, *J. Geophys. Res.*, 92(C12), 12,974–12,978.
- Locarnini, R., A. Mishonov, J. Antonov, T. Boyer, H. Garcia, O. Baranova, M. Zweng, and D. Johnson (2010), *World Ocean Atlas 2009*, vol. 1, *Temperature*, edited by S. Levitus, 184 pp., U.S. Gov. Print. Off., Washington, D. C.
- Lukas, R., and E. Lindstrom (1991), The mixed layer of the western equatorial Pacific Ocean, *J. Geophys. Res.*, 96(S01), 3343–3357.
- McCreary, J. P., W. Han, D. Shankar, and S. R. Shetye (1996), Dynamics of the East India Coastal Current: 2. Numerical solutions, *J. Geophys. Res.*, 101(C6), 13,993–14,010.
- Miller, J. R. (1976), The salinity effect in a mixed layer ocean model, *J. Phys. Oceanogr.*, 6(1), 29–35.
- Morel, A., and D. Antoine (1994), Heating rate within the upper ocean in relation to its bio-optical state, *J. Phys. Oceanogr.*, 24(7), 1652–1665.
- Mukherjee, A., et al. (2014), Observed seasonal and intraseasonal variability of the East India Coastal Current on the continental slope, *J. Earth Syst. Sci.*, 123(6), 1197–1232.
- Murty, V. S. N., Y. V. B. Sarma, D. P. Rao, and C. S. Murty (1992), Water characteristics, mixing and circulation in the Bay of Bengal during southwest monsoon, *J. Mar. Res.*, 50(2), 207–228.
- National Geophysical Data Center (1988), Data announcement 88-MGG-02, Digital relief of the Surface of the Earth, *Natl. Ocean. Atmos. Admin.*, US Dept. Commerce, Boulder, Colo.
- Potemra, J. T., M. E. Luther, and J. J. O'Brien (1991), The seasonal circulation of the upper ocean in the Bay of Bengal, *J. Geophys. Res.*, 96(C7), 12,667–12,683.
- Rao, R. R., and R. Sivakumar (2003), Seasonal variability of sea surface salinity and salt budget of the mixed layer of the north Indian Ocean, *J. Geophys. Res.*, 108(C1), 3009, doi:10.1029/2001JC000907.
- Schiller, A., and J. Godfrey (2003), Indian Ocean intraseasonal variability in an ocean general circulation model, *J. Clim.*, 16(1), 21–39.
- Schiller, R. V., V. H. Kourafalou, P. Hogan, and N. D. Walker (2011), The dynamics of the Mississippi River plume: Impact of topography, wind and offshore forcing on the fate of plume waters, *J. Geophys. Res.*, 116, C06029, doi:10.1029/2010JC006883.
- Sengupta, D., G. N. Bharat Raj, and S. S. Shenoi (2006), Surface freshwater from Bay of Bengal runoff and Indonesian throughflow in the tropical Indian Ocean, *Geophys. Res. Lett.*, 33, L22609, doi:10.1029/2006GL027573.
- Seo, H., S.-P. Xie, R. Murtugudde, M. Jochum, and A. J. Miller (2009), Seasonal effects of Indian ocean freshwater forcing in a regional coupled model*, *J. Clim.*, 22(24), 6577–6596.
- Shankar, D., J. P. McCreary, W. Han, and S. R. Shetye (1996), Dynamics of the East India Coastal Current: 1. Analytic solutions forced by interior Ekman pumping and local alongshore winds, *J. Geophys. Res.*, 101(C6), 13,975–13,991.
- Shankar, D., V. Gopalakrishna, S. Shenoi, F. Durand, S. Shetye, C. Rajan, Z. Johnson, N. Araligidad, and G. Michael (2004), Observational evidence for westward propagation of temperature inversions in the southeastern Arabian Sea, *Geophys. Res. Lett.*, 31, L22609, doi:10.1029/2004GL019652.
- Shenoi, S. S. C., D. Shankar, and S. R. Shetye (2002), Differences in heat budgets of the near-surface Arabian Sea and Bay of Bengal: Implications for the summer monsoon, *J. Geophys. Res.*, 107, 3052, doi:10.1029/2000JC000679.
- Shetye, S. R., S. Shenoi, A. Gouveia, G. Michael, D. Sundar, and G. Nampoothiri (1991), Wind-driven coastal upwelling along the western boundary of the Bay of Bengal during the southwest monsoon, *Cont. Shelf Res.*, 11(11), 1397–1408.
- Shetye, S. R., A. D. Gouveia, S. S. C. Shenoi, D. Sundar, G. S. Michael, and G. Nampoothiri (1993), The western boundary current of the seasonal subtropical gyre in the Bay of Bengal, *J. Geophys. Res.*, 98(C1), 945–954.
- Shetye, S. R., A. D. Gouveia, D. Shankar, S. S. C. Shenoi, P. Vinayachandran, D. Sundar, G. S. Michael, and G. Nampoothiri (1996), Hydrography and circulation in the western Bay of Bengal during the northeast monsoon, *J. Geophys. Res.*, 101(C6), 14,011–14,025.

- Shie, C.-L., K. Hilburn, L. Chiu, R. Adler, I.-I. Lin, E. Nelkin, J. Ardizzone, and S. Gao (2012), *Goddard Satellite-Based Surface Turbulent Fluxes Climatology, Monthly Grid*, version 3, edited by Andrey Savtchenko, Goddard Earth Sci. Data and Inform. Serv. Cent. (GES DISC), Greenbelt, Md., doi:10.5067/MEASURES/GSSTF/DATA309.
- Simmons, H. L., S. R. Jayne, L. C. S. Laurent, and A. J. Weaver (2004), Tidally driven mixing in a numerical model of the ocean general circulation, *Ocean Modell.*, 6(3), 245–263.
- Sindhu, B., I. Suresh, A. Unnikrishnan, N. Bhatkar, S. Neetu, and G. Michael (2007), Improved bathymetric datasets for the shallow water regions in the Indian Ocean, *J. Earth Syst. Sci.*, 116(3), 261–274.
- Smyth, W. D., D. Hebert, and J. N. Moum (1996), Local ocean response to a multiphase westerly wind burst: 2. Thermal and freshwater responses, *J. Geophys. Res.*, 101(C10), 22,513–22,533.
- Sprintall, J., and M. Tomczak (1992), Evidence of the barrier layer in the surface layer of the tropics, *J. Geophys. Res.*, 97(C5), 7305–7316.
- Thadathil, P., V. Gopalakrishna, P. Muraleedharan, G. Reddy, N. Araligidad, and S. Shenoy (2002), Surface layer temperature inversion in the Bay of Bengal, *Deep Sea Res., Part I*, 49(10), 1801–1818.
- Vinayachandran, P. N., and J. Kurian (2007), Hydrographic observations and model simulation of the Bay of Bengal freshwater plume, *Deep Sea Res., Part I*, 54(4), 471–486.
- Vinayachandran, P. N., and S. Mathew (2003), Phytoplankton bloom in the Bay of Bengal during the northeast monsoon and its intensification by cyclones, *Geophys. Res. Lett.*, 30(11), 1572, doi:10.1029/2002GL016717.
- Vinayachandran, P. N., and R. S. Nanjundiah (2009), Indian Ocean sea surface salinity variations in a coupled model, *Clim. Dyn.*, 33(2–3), 245–263.
- Vinayachandran, P. N., and S. R. Shetye (1991), The warm pool in the Indian Ocean, *Proc. Indian Acad. Sci. Earth Planet. Sci.*, 100(2), 165–175.
- Vinayachandran, P., and T. Yamagata (1998), Monsoon response of the sea around Sri Lanka: Generation of thermal domes and anticyclonic vortices, *J. Phys. Oceanogr.*, 28(10), 1946–1960.
- Vinayachandran, P. N., S. R. Shetye, D. Sengupta, and S. Gadgil (1996), Forcing mechanisms of the Bay of Bengal circulation, *Curr. Sci.*, 71(10), 753–763.
- Vinayachandran, P. N., Y. Masumoto, T. Mikawa, and T. Yamagata (1999), Intrusion of the southwest monsoon current into the Bay of Bengal, *J. Geophys. Res.*, 104(C5), 11,077–11,085.
- Vinayachandran, P. N., V. S. N. Murty, and V. Ramesh Babu (2002), Observations of barrier layer formation in the Bay of Bengal during summer monsoon, *J. Geophys. Res.*, 107(C12), 8018, doi:10.1029/2001JC000831.
- Vinayachandran, P. N., T. Kagimoto, Y. Masumoto, P. Chauhan, S. Nayak, and T. Yamagata (2005), Bifurcation of the East India coastal current east of Sri Lanka, *Geophys. Res. Lett.*, 32, L15606, doi:10.1029/2005GL022864.
- Vinayachandran, P. N., D. Shankar, J. Kurian, F. Durand, and S. Shenoi (2007), Arabian Sea mini warm pool and the monsoon onset vortex, *Curr. Sci.*, 93(2), 203–214.
- Vinayachandran, P. N., C. P. Neema, S. Mathew, and R. Remya (2012), Mechanisms of summer intraseasonal sea surface temperature oscillations in the Bay of Bengal, *J. Geophys. Res.*, 117, C01005, doi:10.1029/2011JC007433.
- Vinayachandran, P. N., D. Shankar, S. Vernekar, K. K. Sandeep, P. Amol, C. P. Neema, and A. Chatterjee (2013), A summer monsoon pump to keep the Bay of Bengal salty, *Geophys. Res. Lett.*, 40, 1777–1782, doi:10.1002/grl.50274.
- Vörösmarty, C. J., B. Fekete, and B. A. Tucker (1996), River Discharge Database, Version 1.0 (RivDIS v1.0), vols. 0–6, A contribution to IHP-V Theme 1, Technical Documents in Hydrology Series, technical report, U. N. Educ., Sci., and Cult. Org., Paris.
- Yu, L., and M. J. McPhaden (2011), Ocean preconditioning of cyclone Nargis in the Bay of Bengal: Interaction between Rossby Waves, surface fresh waters, and sea surface temperatures*, *J. Phys. Oceanogr.*, 41(9), 1741–1755.
- Yu, L., J. J. O'Brien, and J. Yang (1991), On the remote forcing of the circulation in the Bay of Bengal, *J. Geophys. Res.*, 96(C11), 20,449–20,454.